Simple, yet stable bearing-only navigation

Tomáš Krajník
Department of Cybernetics
Faculty of Electrical Engineering
Czech Technical University in Prague
121 35 Praha 2, Karlovo náměstí 13, Czech Republic
`tkrajnik@labe.felk.cvut.cz`

Jan Faigl
Department of Cybernetics
Faculty of Electrical Engineering
Czech Technical University in Prague
`xfaigl@labe.felk.cvut.cz`

Vojtěch Vonásek
Department of Cybernetics
Faculty of Electrical Engineering
Czech Technical University in Prague
`vonasek@labe.felk.cvut.cz`

Karel Košnar
Department of Cybernetics
Faculty of Electrical Engineering
Czech Technical University in Prague
`kosnar@labe.felk.cvut.cz`

Miroslav Kulich
Department of Cybernetics
Faculty of Electrical Engineering
Czech Technical University in Prague
`kulich@labe.felk.cvut.cz`

Libor Přeučil
Department of Cybernetics
Faculty of Electrical Engineering
Czech Technical University in Prague
`preucil@labe.felk.cvut.cz`

Abstract

This article describes a simple monocular navigation system for a mobile robot based on the map-and-replay technique. The presented method is robust, easy to implement, does not require sensor calibration or structured environment and its computational complexity is independent of the environment size. The method can navigate a robot while sensing only one landmark at a time, making it more robust than other monocular approaches. The aforementioned properties of the method allow even low-cost robots to effectively act in large outdoor and indoor environments with natural landmarks only.

The basic idea is to utilize a monocular vision to correct only the robot's heading and leaving distance measurements just to the odometry. The heading correction itself can suppress the odometric error and prevent the overall position error from diverging.

The influence of a map-based heading estimation and odometric errors on the overall position uncertainty is examined. A claim that for closed polygonal trajectories the position error of this type of navigation does not diverge is stated. The claim is defended mathematically and experimentally. The method has been experimentally tested in a set of indoor and outdoor experiments, during which the average position errors have been lower than 0.3 m for paths over 1 km long.

1 Introduction

The fundamental problem of mobile robotics is to autonomously navigate a mobile robot along a given path. To fulfill this task efficiently, a robot should maintain some knowledge about its surrounding environment, especially its position relative to the path or desired destination. Such knowledge may be represented in a form of a map, which can be used to estimate the robot position as well as for the motion planning. The map is either known a priory and the robot performs localization, or is created on-line and the mobile robot performs so-called Simultaneous Localization and Mapping (SLAM).

The solid mathematical background of the Kalman filter (Kalman, 1960) allowed the research community to establish a sufficient theoretical framework for EKF-based SLAM. Proof of EKF convergence (Dissanayake et al., 2001) and lower bounds (Gibbens et al., 2000) on the robot position uncertainty have been formulated. Upper bounds are discussed in the paper (Mourikis and Roumeliotis, 2004), where authors emphasize the importance of robot heading precision during the mapping process. To our knowledge, there is no other paper concerning upper bounds of EKF position estimation. Unfortunately, optimality of the Kalman filter is proven only for linear systems and therefore the main weakness of EKF methods lies in the linearization. The papers (Julier and Uhlmann, 2001; Martinelli et al., 2005) indicate that due to errors introduced in linearization EKF methods might provide inconsistent results. Although the linearization process poses a significant threat to the consistency of the position estimation, it can be elegantly avoided using the inverse depth representation (Montiel et al., 2006; Civera et al., 2008).

1.1 Vision-based navigation

The theoretical solutions of bearing-only SLAM have gained importance as the computational power of nowadays computers allow real-time image processing. The nature of visual information allows to build sparse maps from well distinguishable landmarks (Lowe, 1999; Lowe, 2004), which are relatively easy to register. However, the range information is not provided directly by standard cameras. Some bearing-only methods use stereovision in order to obtain immediate range information (Kidono et al., 2000). Other methods substitute stereovision by motion and use a single monocular camera (Davison et al., 2007; Holmes et al., 2008; Montiel et al., 2006).

Most monocular approaches are computationally complex and achieve low operational speeds when mapping large scale environments. This problem can be solved by dividing the large global map to smaller maps with mutual position information (Estrada et al., 2005; Clemente et al., 2007; Bosse et al., 2004; Williams et al., 2009).

A different approach is to build an environment map in advance and then use the map for localization (Blanc et al., 2005; Matsumoto et al., 1996; Royer et al., 2007; Chen and Birchfield, 2009; Segvic et al., 2007). In the article (Royer et al., 2007), a monocular camera is carried through an environment and a video is recorded. The recorded video is then processed (in a matter of several minutes) and subsequently used to guide a mobile robot along the same trajectory. Authors (Chen and Birchfield, 2006; Chen and Birchfield, 2009) present an even simpler form of navigation in a learned map. Their method utilizes a map consisting of salient image features remembered during a teleoperated drive. The map is divided into several conjoined segments, each associated with a set of visual features detected along it and a milestone image indicating the segment end. When a robot navigates a segment, its steering commands are calculated from positions of currently recognized and remembered features. The robot using this method moves forward with a constant speed and steers right or left with a constant velocity or does not steer at all. In the paper (Chen and Birchfield, 2006), the segment end was detected by means of comparing the milestone image with the current view. The improved version (Chen and Birchfield, 2009) of the qualitative navigation uses a more sophisticated method to determine the segment end. The method takes into account the odometry, the current heading and the similarity of the current and the milestone image. Still, the authors mention some problems with detection of the segment end. We claim that the segment end can be detected solely by the odometry and the comparison with the milestone image is not always necessary. Comparison with the milestone image increases robustness of the navigation method in cases of wheel slippage and other odometry errors.

The map-and-replay approach is closely related to the visual servoing, in which the control of a robot is based on visual measurements (Chaumette and Hutchinson, 2006; Chaumette and Hutchinson, 2007). Control inputs are either computed directly by a comparison of the current and reference image (Remazeilles and Chaumette, 2007; Segvic et al., 2009) or by a computation of camera coordinates in the world reference frame (Wilson et al., 1996; DeMenthon and Davis, 1992). Normally, the visual servoing relies on a geometrical approach to calculate relations of map landmarks to the current image salient points (Segvic et al., 2009). These relations are used to calculate an interaction matrix (Chaumette and Hutchinson, 2006), which links observations to control inputs of the robot. The robot's control input can be computed from the Jacobian (Burschka and Hager, 2001), which relates world and image points, or from homography or fundamental matrices (Guerrero et al., 2005; Remazeilles and Chaumette, 2007), which relate coordinates between actual and reference images. A strong reliance on the geometrical representation either requires camera calibration (Burschka and Hager, 2001; Remazeilles and Chaumette, 2007; Segvic et al., 2009) or structured environment (Guerrero et al., 2005; Remazeilles and Chaumette, 2007). A more detailed overview of visual servoing approaches related to the field of mobile robotics is presented in (Chen and Birchfield, 2009; Segvic et al., 2009). Contrary to the visual servoing approach, our method does not require a calibrated camera and does not rely on the environment structure.

1.2 Motivation

The target of our efforts is to create a system, which would be able to reliably navigate a mobile robot in an unstructured environment of any size. To achieve this challenging goal, we have decided that the navigation system should have the following properties:

- scalability - its computational complexity should be independent of the environment size,
- simplicity - the method should be as simple as possible, because complex systems are more likely to contain errors,
- swiftness - it has to satisfy real-time constraints,
- standardness - it should use off-the shelf equipment,
- stability - the position uncertainty should not diverge with time.

The basic idea of the map-and-replay technique is similar to the industrial practice of programming stationary robots. One of the basic methods to program a stationary robot is by means of (tele)operation. A skilled operator guides the tip of the robot arm in order to perform a certain task (e.g. painting, welding). The robot records signals from its build-in receptors - typically incremental rotation sensors at its joints. During the robot operation, the recorded sequences serve as inputs for the robots' controllers. Though well established and efficient, this method is not applicable to mobile robots in unstructured environments due to the uncertainty in the robot-environment interaction. A typical example of the case would be the use of the odometry in a mobile robot localization - the uncertainty caused by wheel slippages tends to accumulate, which does not make the odometry suitable for long-term localization and navigation. To effectively cope with the uncertainty in robot's position, a mobile robot must use exteroreceptors to sense the surrounding environment. A mobile robot position and its heading can be estimated through measurements of the surrounding environment.

Several authors of SLAM algorithms acknowledge the fact, that the uncertainty of robot heading is a crucial factor affecting the quality of the map and subsequently the quality of position estimation in the localization step. The influence of the heading estimation has been evaluated both theoretically and practically (Frese, 2006). We extend the idea of the heading estimation importance and claim that for long term mobile robot localization it is sufficient to use exteroceptive sensors for the heading estimation and the Cartesian coordinates estimation can be based just on proprioceptive sensors.

1.3 Paper overview

A minimalistic approach to monocular localization and mapping is presented in this paper. We claim, that for the navigation in a known environment, a robot needs a map just to estimate its heading and can measure its position by the odometry. Formulating this particular instance of the navigation mathematically, we provide a formal proof of this claim. Furthermore, several large outdoor experiments confirm the expected system performance. We think that the most important contribution of our paper is not the presented method, but the convergence proof presented in Section 3. The proof would apply to several (Zhang and Kleeman, 2009; Guerrero et al., 2005; Chen and Birchfield, 2009) other methods, which use vision to correct heading and lateral position errors.

The rest of this paper is organized as follows. The proposed minimalistic navigation method is described in the next section. A mathematical model of this navigation method is outlined and its properties are examined in Section 3. A theorem, which claims that this method prevents position uncertainty divergence is formulated and proven in the same section. The theoretical analysis is followed by a discussion on practical issues of the navigation method. Experimental results verifying, whether the system retains the expected properties, are described in Section 5. A conclusion resumes the paper and shortly discusses properties of the proposed navigation method and outlines possible future improvements.

2 Navigation system description

The proposed navigation procedure is based on the map-and-replay technique. The idea is simple, a robot is manually driven through an environment and creates a map of its surrounding environment. After that, the map is used for the autonomous navigation. A similar technique for autonomous navigation based on computation of a robot steering from positions of remembered features has been described in (Chen and Birchfield, 2006; Royer et al., 2007; Zhang and Kleeman, 2009). To minimize the robot sensor equipment and to satisfy the “standardness” property mentioned in Section 1.2 we consider the most available sensors. The fundamental navigation property of a mobile vehicle is the traveled distance, which can be estimated by an odometry. The odometric error is cumulative, and therefore can be considered precise only in a short term. Another standard available sensor, which does not require additional infrastructure, is a compass. A fusion of data from the compass and the odometry can provide position estimation, but is still unsuitable for long-term navigation, because it lacks sufficient feedback from the robot’s surrounding environment. To increase robot ability to sense the environment, one of the most advantageous sensors is a camera, which can provide lots of information.

Using these three main sensors, we have proposed the following simple navigation strategy:

- The robot is navigated along a sequence of straight line segments.
- At each segment start, the robot is turned to a direction according to the compass value.
- The steering control along the straight segment is computed from matched visual features providing a so-called visual compass.
- The end of each segment is recognized according to the traveled distance, which is measured by the odometry.

The crucial component of the proposed navigation procedure is a map, which is created by guiding the robot along a path consisting of straight line segments. Each segment has its own landmark map L_i, consisting of salient features detected in images captured by the robot's forward looking camera, the initial robot orientation α and the segment length s. Once the map is created, the robot can travel autonomously within the mapped environment. During the navigation along a segment, the robot establishes correspondences of the currently seen and previously mapped landmarks and computes differences in the expected and recognized positions for each such correspondence. The robot steers in a direction that reduces those differences while moving straight at a constant speed until its odometry indicates that the current segment has been traversed. At the end of the segment the robot switches to the next learned segment, turns to a direction of the initial orientation of the segment and traverses the segment while keeping its direction according to matched features.

The next section describes the robot equipment and image processing. The algorithm for the map creation during learning phase is described in Section 2.2 and the navigation algorithm is depicted in Section 2.3.

2.1 Robot equipment

The proposed method has been verified on the P3AT robot with the Unibrain Fire-i601c camera, the TCM2 compass and the HP 8710p laptop, see Figure 1a. At first, the camera was equipped with a 7 mm objective with an electronically-driven iris to prevent sunlight dazzle. The objective has been replaced by a new one with a 4.5 mm focus length in year 2008. At the same time, electronically-driven iris has been substituted by a software exposure control. The laptop has Core2 Duo CPU running at 2.00GHz and 1 GB of memory. Image processing is computationally demanding and therefore the additional UPC70 battery had been used for longer experiments. To increase the robot action radius, the three original batteries (connected in parallel) were replaced by one high-capacity battery and the robot's internal PC has been disabled. The navigation system has been implemented in C/C++ as a standalone Linux application.

The Image Processing algorithm is a critical component of the navigation system. The vision system must provide enough information to steer the robot in the right direction. Furthermore, it should be robust to real world conditions, i.e. changing illumination, minor environment changes and partial occlusions and of course its performance should allow the real-time response.

We have decided to use the Speeded Up Robust Features (SURF) (Bay et al., 2006) to identify landmarks in the image. The SURF method is reported to perform better than most SIFT (Lowe, 1999) implementations in terms of speed and robustness to viewpoint and illumination changes. To achieve an additional speedup the CPU implementation of the algorithm has been adjusted to use both processor cores for parallel image processing. The captured image is horizontally divided and both parts are processed in parallel. Later on, we switched to the GPU (Cornelis and Gool, 2008) version of the algorithm. The GPU version has better real-time performance, but is less distinctive than the CPU implementation (Svab et al., 2009). Normally, the recognition of a 1024x768 grayscale image provides descriptors of 150-300 features and takes 100-500 ms. The outdoor environment is usually richer in detected features and image processing tends to be slower than indoors. The algorithm provides image coordinates of the salient features together with their descriptions. A typical outdoor processed image with highlighted feature positions is shown in Figure 1b.

2.2 Learning phase

In the learning phase, the robot is manually guided through an environment in a turn-move manner and creates a map consisting of several straight segments. Each segment is described by its length s, its azimuth α and a set of detected landmarks L. A landmark $l \in L$ is described by the tuple $(\mathbf{e}, k, \mathbf{u}, \mathbf{v}, f, g)$, where $\mathbf{e}$ is the SURF descriptor and k indicates the number of images, in which the landmark was detected. Vectors $\mathbf{u}$ and $\mathbf{v}$ denote positions of the landmark in the captured image at the moment of its first and last detection and f and g are the distances of the robot from the segment start in these moments.

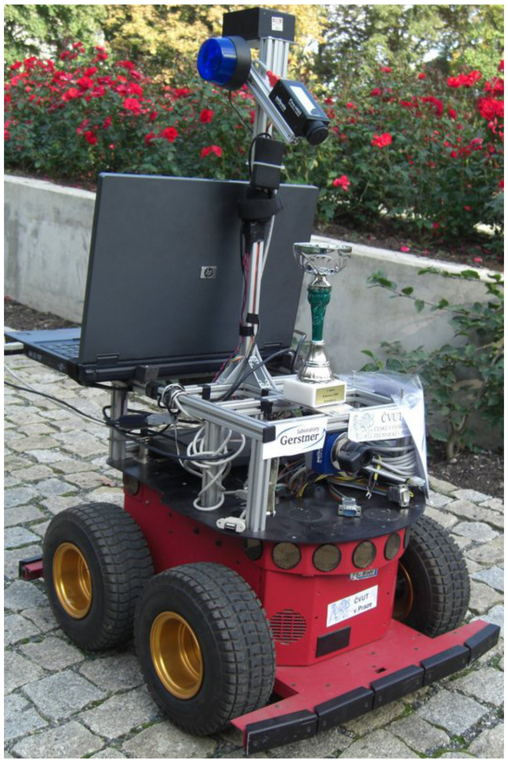

(a) Robot configuration for experiments.

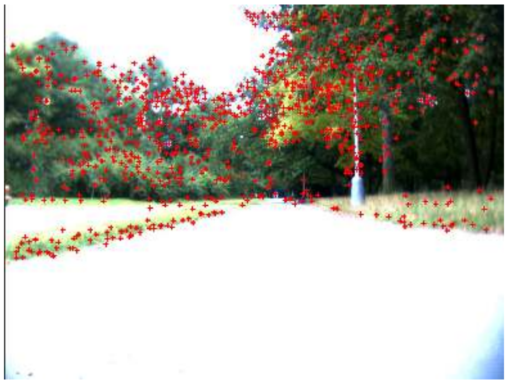

(b) Image captured by robot camera and detected SURF positions.

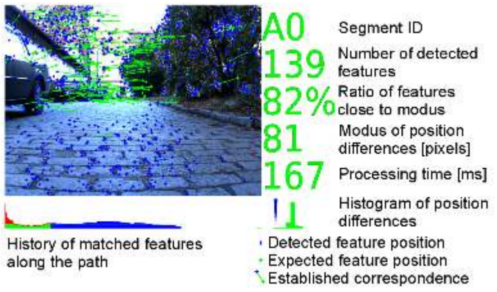
A0
Segment ID
139
Number of detected features
82%
Ratio of features close to modus
81
Modus of position differences [pixels]
167
Processing time [ms]
Histogram of position differences
History of matched features along the path
Detected feature position
Expected feature position
Established correspondence

(c) Robot GUI with navigation phase data.

Figure 1: Robot platform, detected features and navigation GUI.

The procedure that creates a map of one segment is shown in Algorithm 1. Before the robot starts to learn a segment, it reads compass data to establish the segment azimuth α and resets its odometric counters. After that, the robot starts to move forwards, tracks detected features and inserts them to the set L until the operator requests to stop. Images are continuously captured and processed during the movement. For each currently tracked landmark $\boldsymbol{t_i}$ (from the set T) two of the best matching features from the set of new features are found. If these two pairs are distinguishable enough (Bay et al., 2006) the best matching feature is associated to the tracked landmark, which is updated (values k, v, g). Each new feature is added to the set of tracked landmarks T and its u and v are set to the value of the current distance from the segment start and the counter of the feature detection k is set to one. The segment description is saved at the end of the segment and the operator can turn the robot to another direction and initiate mapping of a new segment. The format of the file, which stores the segment description, is shown in Table 1.

2.3 Autonomous Navigation Mode

In the autonomous navigation mode an operator enters a sequence of segments and indicates, whether the robot should travel repeatedly or not. The robot is placed at the start of the first segment, loads the description of the segment and turns itself to the segment azimuth and starts moving forwards. The navigation procedure is shown in Algorithm 2. The relevant landmarks for the current robot position (i.e. according to the distance from the segment start) are selected from the set of the learned landmarks L. Correspondences between the mapped and the currently detected landmarks are established in the same way as in the learning phase. A difference in horizontal image coordinates of the features is computed for each such couple. A modus of those differences is estimated by the histogram voting method. The modus is converted to a correction value of the movement direction, which is reported to the robot's steering controller. After the robot travels distance greater or equal to the length of the given segment, the next

Algorithm 1: Learn one segment

Input: α – an initial robot orientation (compass value)

Output: (α, s, L) – the data associated to the segment, where s is the traveled distance and L is a set of landmarks, a landmark is the tuple (k, e, u, v, f, g), where e is the SURF descriptor, k is a counter of feature detection, u and v are positions of the features in the image (at the moment of their first, resp. last occurrence), f and g denote distance from the segment start according to u, resp. v.

```
$L \leftarrow \emptyset$                                   // a set of learned landmarks
$T \leftarrow \emptyset$                                   // a set of tracked landmarks
$\alpha \leftarrow$ compass value          // a robot orientation at the beginning of segment learning
repeat
    $d \leftarrow$ current distance from the segment start
    $S \leftarrow$ extracted features with associated image position, $(u,e) \in S$, $u$ position, $e$ feature descriptor
    foreach $\boldsymbol{t_i} = (e_i, k_i, u_i, v_i, f_i, g_i) \in T$ do
        $(u_a, e_a) \leftarrow \mathrm{argmin}\{||e_i, e(s)|| \,|s \in S\}$   // select the best matching descriptor from $S$ to $e_i$
        $(u_b, e_b) \leftarrow \mathrm{argmin}\{||e_i, e(s)|| \,|s \in S \setminus \{(u_a, e_a)\}\}$// select the next best matching descriptor
        if $||(e_i, e_a)|| \ll ||(e_i, e_b)||$ then
            $\boldsymbol{t_i} \leftarrow (e_i, k_i + 1, u_i, u_a, f_i, d)$              // update matched landmark
            $S \leftarrow S \setminus \{(u_a, e_a)\}$      // remove matched feature from the current set of detected features
        else
            $T \leftarrow T \setminus \{\boldsymbol{t_i}\}$                // remove $\boldsymbol{t_i}$ from the set of tracked landmarks
            $L \leftarrow L \cup \{\boldsymbol{t_i}\}$                    // add $\boldsymbol{t_i}$ to the set of learned landmarks
    foreach $(u, e) \in S$ do
        $T \leftarrow T \cup \{(e, 1, u, u, d, d)\}$          // add new feature to the set of tracked landmarks
until operator terminates learning mode
$s \leftarrow d$                                 // the total traveled distance along the segment
$L \leftarrow L \cup T$           // add the current tracked landmarks to the set of learned landmarks
```

Table 1: A part of a segment map in a text file

Record	Value	Meaning
Initial azimuth and length:	2.13, 7.03	α, s
Landmark 0:		
First position:	760.74, 163.29	$\mathbf{u_{l_0}}$
Last position:	894.58, 54.44	$\mathbf{v_{l_0}}$
Max visibility:	128	k_{l_0}
First and last visible distance:	0.00, 4.25	f_{l_0}, g_{l_0}
Descriptor:	1,0.116727,-0.000254,0.000499,0.000352,...	$\mathbf{e_{l_0}}$
Landmark 1:		
First position:	593.32, 381.17	$\mathbf{u_{l_1}}$
Last position:	689.89, 377.23	$\mathbf{v_{l_1}}$
Max visibility:	125	k_{l_1}
First and last visible distance:	0.00, 6.73	f_{l_1}, g_{l_1}
Descriptor:	-1,0.070294,-0.006383,0.012498,0.006383,...	$\mathbf{e_{l_1}}$

segment description is loaded and the procedure is repeated. During the navigation, the robot displays the relevant states (mapped and recognized landmarks, recognition success ratio etc.) on its graphical interface, see Figure 1c.

Algorithm 2: Traverse one segment

Input: (α, s, L) – the data associated to the segment, where α is an initial angle of the robot orientation at the segment start, s is the traveled distance and L is a set of landmarks, a landmark is the tuple (e, k, u, v, f, g), where e is a SURF descriptor, k is a counter of feature detection, u and v are positions of feature in the image (at the moment of the first, resp. last, occurrence), f and g denote distances from the segment start according to u, resp. v.

Output: ω – a steering speed

```
turn(α)                                                   // turn robot in the direction α
d ← current distance from the segment start
while $d < s$ do
    $T \leftarrow \emptyset$                              // a set of current tracked landmarks
    $H \leftarrow \emptyset$   // a set of differences (horizontal position in the image) of matched features
    $d \leftarrow$ current distance from the segment start
    $S \leftarrow$ extracted features with associated image position, $(u, e) \in S$, $u$ position, $e$ feature descriptor
    foreach $\boldsymbol{l_i} = (e_i, k_i, u_i, v_i, f_i, g_i) \in L$ do
        if $f_i \geq d \geq g_i$ then
            $T \leftarrow T \cup \{\boldsymbol{l_i}\}$   // add landmark to the tracked landmarks according to the traveled distance
    while $|T| > 0$ do
        $(e_i, k_i, u_i, v_i, f_i, g_i) \leftarrow \mathrm{argmax}_{\boldsymbol{t} \in T}\, k(\boldsymbol{t})$ // get landmark with maximal number of occurrences $k$
        $(u_a, e_a) \leftarrow \mathrm{argmin}\{||e_i, e(s)||\ |s \in S\}$   // select the best matching descriptor from $S$ to $e_i$
        $(u_b, e_b) \leftarrow \mathrm{argmin}\{||e_i, e(s)||\ |s \in S \setminus \{(u_a, e_a)\}\}$ // select the next best matching descriptor
        if $||(e_i, e_a)|| \ll ||(e_i, e_b)||$ then
            $p \leftarrow \frac{|v_i - u_i|}{|g_i - f_i|}(d - f_i) + u_i - u_a$   // estimate angle to the matched landmark
            $H \leftarrow H \cup \{p\}$                   // add horizontal difference to set of differences
        $T \leftarrow T \setminus \{(e_i, k_i, u_i, v_i, f_i, g_i)\}$   // discard used landmark
    $\omega \leftarrow \mathrm{modus}(H)$                 // determine new robot steering velocity
    report $\omega$ to steering controller
```

An important aspect of this navigation algorithm is the fact that it does not need to explicitly localize the robot or to create a three-dimensional map of detected landmarks. It should also be noted that the proposed method is able to work in real-time. Even though the camera readings are utilized only to correct the robot direction and the distance is measured by the imprecise odometry, the position uncertainty does not accumulate if the robot changes direction often enough. The stability of the proposed navigation method is discussed in the next section.

3 Stability of bearing-only navigation

At first, we describe in an informal way how the robot position uncertainty is changed as the robot travels a closed path. That should help to interpret mathematical formalism describing the robot position uncertainty in geometrical terms and make the rest of this chapter more comprehensible. After that, we lay down a formal description of the proposed navigation method and analyze its stability. We outline a model of the robot movement, and depict equations allowing the computation of the robot position uncertainty. Next, we use these equations to compute the robot position uncertainty for a closed path. Finally, we examine properties of the proposed model and establish conditions ensuring that the robot position error does not diverge.

3.1 Geometrical interpretation

Suppose the learned path is a square and the robot has to travel it repeatedly. The robot is placed at a random (2D Gaussian distribution with zero mean) position near to the first segment start, see Figure 2. The initial position uncertainty can be therefore displayed as a circle, in which the robot is found with 90% probability. The navigation procedure is executed and the robot starts to move along the first segment. Because it senses landmarks along the segment and corrects its heading, its lateral position deviation is decreased. However, due to the odometric error, the longitudal position error increases. At the end of the segment, the circle denoting position uncertainty becomes an ellipse with a shorter axis perpendicular to the segment. Heading corrections are dependent on the value of the lateral deviation (see Section 3.2), the greater the deviation, the stronger the effect of heading corrections and therefore the lateral error decreases by a factor h for every traversed segment. The odometry error is independent of the current position deviation and is affected only by the length of the traversed segment and therefore it can be modeled as an additive error o.

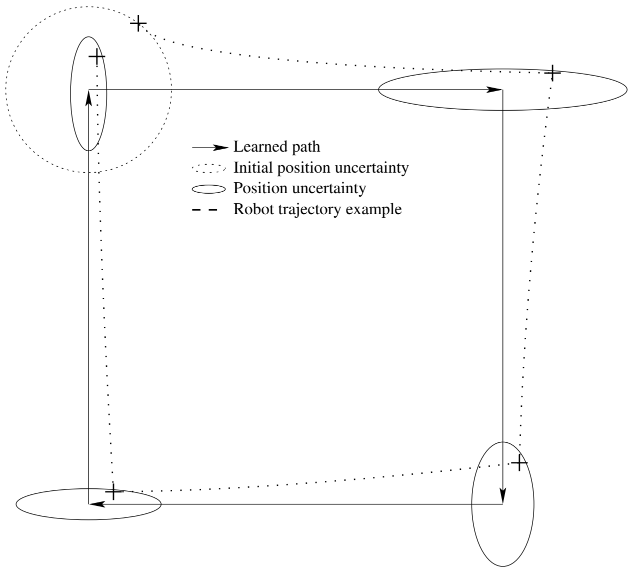

Figure 2: Position uncertainty evolution for a simple symmetric path.

After the segment is traversed, the robot turns by 90° and starts to move along the next segment. The uncertainty changes again, but because of the direction change, the longer ellipse axis shrinks and the shorter is elonged due to the odometry error. This repeats for every traversed segment, the size of the uncertainty ellipse converges to a finite value. Since this particular trajectory is symmetric, axes lengths a, b of the "final" ellipse can be easily computed by the equations

$$\begin{aligned} a &= hb \\ b &= a + o, \end{aligned} \tag{1}$$

where h is the coefficient of the lateral error reduction and o is the odometric error. The position error for $o = 1$ and $h = 0.25$ is shown in Figure 2. Though simple, this particular symmetric case gives us a basic insight into the problem. Now we will derive a broader mathematical model of the navigation, examine its properties and show that the uncertainty does not diverge for nonsymmetrical trajectories as well.

3.2 Navigation

The proposed navigation method is based on the following assumptions:

- the robot moves in a plane,
- the map already exists in a form of a sequence of conjoined linear segments with landmark description,
- at least two segments of the mapped path are not collinear,
- the robot can recognize and associate a nonempty subset of mapped landmarks and determine their bearing,
- the robot can (imprecisely) measure the traveled distance by the odometry,
- the camera is aimed forward, i.e. in the direction of the robot movement.

The path P consists of a sequence of linear segments p_i. The robot moves in a plane, i.e. its state vector is (x, y, φ). The robot we consider has a differential, nonholonomic drive and therefore $\dot{x} = v\cos(\varphi)$ and $\dot{y} = v\sin(\varphi)$. For each segment p_i, there exists a nonempty subset of landmarks and a mapping between the robot position and the expected bearing of each landmark is established. At the start of each segment, the robot resets its odometry counter and turns approximately towards the segment end to sense at least one of the segment landmarks. The robot establishes correspondences of seen and mapped landmarks and computes differences in expected and recognized bearings. The robot steers in a direction that reduces those differences while moving forward until its odometry indicates that the current segment has been traversed.

Definition 1 (Closed path stability property) *Assume a robot navigates a closed path several times. Furthermore the robot is using an environment map only for heading corrections and measuring the distance by the odometry. Then a path for which the robot position uncertainty does not diverge has the closed path stability property.*

Theorem 1 *A path consisting of several conjoined segments retains the closed path stability property if the assumptions in Section 3.2 are satisfied.*

3.3 Movement along one segment

At first, let us examine how a robot moves along one segment. We will focus on the position before and after traversing one segment and establish mapping from the robot position error at the segment start to the robot position error at the segment end.

To keep the model simple, we assume, that the robot as well as the landmarks are positioned in a plane. We will consider having a map consisting of a single segment of length s with d landmarks, with positions represented as vectors $\mathbf{u_i}$. Since the robot is equipped with a forward-heading camera, learned landmark positions $\mathbf{u_i}$ are not assumed to be distributed uniformly along the path, but rather shifted in the direction of the robot movement by a distance ρ. We can assume, that $\rho \approx \frac{1}{d}\sum_{i=0}^{d-1} u_x i$, where d is the number of mapped landmarks. Let us place the segment start at the coordinate origin and the segment end at the position $[s, 0]^T$. We designate the robot position prior to the segment traversal as $\mathbf{a} = [a_x, a_y]^T$ and the final robot position as $\mathbf{b} = [b_x, b_y]^T$, see Figure 3. Let us assume that at every moment during the segment traversal the robot recognizes a non-empty subset $\mathbf{W}$ of previously learned landmarks and the robot heads in a direction, which minimizes the horizontal deviation of expected and recognized landmark positions. We denote the intersection of robot heading with the learned segment axis as $\mathbf{w}$. At the beginning of the segment

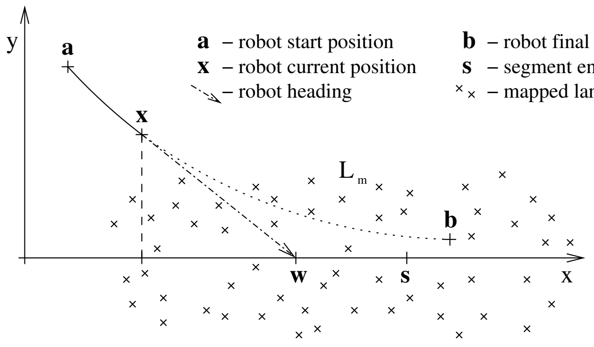

Figure 3: Robot movement model for a single path segment.

traversal, this position equals approximately $[\rho, 0]^T$ (i.e. $\mathbf{w} \approx [\rho, 0]^T$). As the robot traverses the segment, it loses sight of nearby landmarks and recognizes new ones. As new, more distant landmarks appear in the robot field of view and nearby landmarks disappear, the set $\mathbf{W}$ changes and the point $\mathbf{w}$ moves along the segment. It can be assumed that the point $\mathbf{w}$ moves approximately at the speed of the robot and therefore it is always ahead of the robot by the distance ρ.

Based on these premises, the robot position $[x, y]^T$ in terms of $y = f(x)$ can be established. The robot movement can be characterized by the following differential equation:

$$\frac{dx}{dy} = \frac{\rho}{-y}. \tag{2}$$

Solving (2) gives us a trajectory, along which the robot moves:

$$y = ce^{-\frac{x}{\rho}}.$$

Considering a boundary condition $a_y = f(a_x)$, the constant c equals to

$$c = \frac{a_y}{e^{-\frac{a_x}{\rho}}}.$$

Considering that the range of robot's sensor is higher than the robot position uncertainty and that the segment length is higher than the robot lateral distance from the segment start, (i.e. $\rho \gg a_x$, $s \gg |a_y|$), the constant c equals approximately a_y and the traveled distance is approximately equal to the segment length. Therefore, we can estimate the robot position after traveling a segment of length s by the following equations:

$$\begin{aligned} b_x &= a_x + s, \\ b_y &= a_y e^{-\frac{s}{\rho}}. \end{aligned} \tag{3}$$

We can transform (3) to the matrix form

$$\begin{pmatrix} b_x \\ b_y \end{pmatrix} = \begin{pmatrix} 1 & 0 \\ 0 & e^{-\frac{s}{\rho}} \end{pmatrix} \begin{pmatrix} a_x \\ a_y \end{pmatrix} + \begin{pmatrix} s \\ 0 \end{pmatrix}. \tag{4}$$

Equation 4 is valid for an error-free odometry. If the odometry error is modeled as a multiplicative uncertainty, the equation changes to

$$\left(\begin{array}{c} b_x \\ b_y \end{array}\right) = \left(\begin{array}{cc} 1 & 0 \\ 0 & e^{-\frac{s}{\rho}} \end{array}\right)\left(\begin{array}{c} a_x \\ a_y \end{array}\right) + s\left(\begin{array}{c} 1+\upsilon \\ 0 \end{array}\right), \tag{5}$$

where υ is a random variable drawn from the Gaussian distribution with the zero mean and the variance ϵ. Accounting the heading sensor noise, equation (5) changes to

$$\left(\begin{array}{c} b_x \\ b_y \end{array}\right) = \left(\begin{array}{cc} 1 & 0 \\ 0 & e^{-\frac{s}{\rho}} \end{array}\right)\left(\begin{array}{c} a_x \\ a_y \end{array}\right) + \left(\begin{array}{c} s+s\upsilon \\ \xi \end{array}\right), \tag{6}$$

where ξ is a random variable of the Gaussian distribution with the zero mean and the variance τ. Consolidating the previous equation (6), we can state

$$\mathbf{b} = \mathbf{Ma} + \mathbf{s}.$$

The aforementioned movement model holds for a segment aligned with the x-axis. For a segment with an arbitrary orientation α, the movement model becomes

$$\mathbf{b} = \mathbf{R^T MRa} + \mathbf{R^T s}, \tag{7}$$

where

$$\mathbf{R} = \left(\begin{array}{cc} \cos\alpha & -\sin\alpha \\ \sin\alpha & \cos\alpha \end{array}\right), \qquad \mathbf{M} = \left(\begin{array}{cc} 1 & 0 \\ 0 & e^{-\frac{s}{\rho}} \end{array}\right) = \left(\begin{array}{cc} 1 & 0 \\ 0 & m \end{array}\right).$$

Equation (7) corresponds to aligning the segment with the x-axis, applying $\mathbf{M}$, adding the odometric and the sensor noise and rotating the segment back to the direction α. In the following text, we use $\mathbf{N} = \mathbf{R^T MR}$, which shortens equation (7) to

$$\mathbf{b} = \mathbf{Na} + \mathbf{R^T s}. \tag{8}$$

All the aforementioned assumptions about the surrounding environment (landmark shift equal to ρ, $\rho \gg a_x$ etc.) can be relaxed as long as $m < 1$ for $s > 0$.

3.4 Position uncertainty

Now, the dependence of the robot position uncertainty at the segment end to its uncertainty at the segment start can be examined. Consider that the robot position $\mathbf{a}$ before the segment traversal is a random variable drawn from a two-dimensional normal distribution with the mean $\hat{\mathbf{a}}$ and the covariance matrix $\mathbf{A}$. To compute the robot position uncertainty after the segment traversal, we apply equation (8) to $\mathbf{a}$. Since the robot movement model in equation (8) has only linear and absolute terms, the robot position uncertainty after the segment traversal will constitute a normal distribution with the mean $\hat{\mathbf{b}}$ and the covariance matrix $\mathbf{B}$.

We denote $\mathbf{a} = \hat{\mathbf{a}} + \tilde{\mathbf{a}}$, where $\hat{\mathbf{a}}$ is the mean of $\mathbf{a}$ and $\tilde{\mathbf{a}}$ is a random variable of a normal distribution with the zero mean and the covariance $\mathbf{A}$. Similarly, we can denote $\mathbf{b} = \hat{\mathbf{b}} + \tilde{\mathbf{b}}$. Thus, we can rewrite equation (7) as follows

$$\tilde{\mathbf{b}} = \mathbf{R^T MR}\tilde{\mathbf{a}} + \mathbf{R^T}\tilde{\mathbf{s}}.$$

We can claim, that

$$\tilde{\mathbf{b}}\tilde{\mathbf{b}}^\mathbf{T} = (\mathbf{R^T MR}\tilde{\mathbf{a}} + \mathbf{R^T}\tilde{\mathbf{s}})(\mathbf{R^T MR}\tilde{\mathbf{a}} + \mathbf{R^T}\tilde{\mathbf{s}})^\mathbf{T}.$$

Since $\tilde{\mathbf{s}}$ and $\tilde{\mathbf{a}}$ are independent and do not correlate,

$$\tilde{\mathbf{b}}\tilde{\mathbf{b}}^\mathbf{T} = \mathbf{R^T MR}\tilde{\mathbf{a}}\tilde{\mathbf{a}}^\mathbf{T}\mathbf{R^T M^T R} + \mathbf{R^T}\tilde{\mathbf{s}}\tilde{\mathbf{s}}^\mathbf{T}\mathbf{R},$$

which rewritten in terms of covariance matrices is

$$\mathbf{B} = \mathbf{R^T M R A R^T M^T R} + \mathbf{R^T S R}, \tag{9}$$

where

$$\mathbf{S} = \begin{pmatrix} s^2\epsilon^2 & 0 \\ 0 & \tau^2 \end{pmatrix}.$$

Equation (9) allows us to compute the robot position uncertainty after traversing one segment.

3.5 Traversing multiple segments

Let us consider a path consisting of n chained segments denoted by $i \in \{0, \ldots, n-1\}$ with the end of the last segment equal to the start of the first segment, i.e. the considered path is closed. We denote length and orientation of the i^{th} segment as s_i and α_i. The robot position before and after traversing the i^{th} segment is noted as $\mathbf{a_i}$ and $\mathbf{b_i}$. Since the robot position at the end of the i^{th} segment equals to its start position at the segment $i+1$, we can state that $\mathbf{a_{i+1}} = \mathbf{b_i}$.

The movement model (9) for the i^{th} traveled segment is

$$\mathbf{A_{i+1}} = \mathbf{B_i} = \mathbf{R_i^T M_i R_i A_i R_i^T M_i^T R_i} + \mathbf{R_i^T S_i R_i} \tag{10}$$

Considering $\mathbf{N_i} = \mathbf{R_i^T M_i R_i}$ and defining $\mathbf{T_i} = \mathbf{R_i^T S_i R_i}$, we can rewrite (10) as

$$\mathbf{A_{i+1}} = \mathbf{N_i A_i N_i^T} + \mathbf{T_i}.$$

One can compute the robot position uncertainty in terms of the covariance matrix after traversing i path segments in the following terms:

$$\mathbf{A_i} = \left(\prod_{\mathbf{j=i-1}}^{\mathbf{0}} \mathbf{N_j}\right) \mathbf{A_0} \left(\prod_{\mathbf{j=0}}^{\mathbf{i-1}} \mathbf{N_j^T}\right) + \sum_{\mathbf{j=0}}^{\mathbf{i-1}} \left(\left(\prod_{\mathbf{k=i-1}}^{\mathbf{j}} \mathbf{N_k}\right) \mathbf{N_j^{-1} T_j} \left(\mathbf{N_j^T}\right)^{-1} \left(\prod_{\mathbf{k=j}}^{\mathbf{i-1}} \mathbf{N_k^T}\right)\right). \tag{11}$$

To examine, how the robot position uncertainty changes after the robot travels the entire learned path i-times we define $\mathbf{C_i} = \mathbf{A_{in}}$ (e.g. $\mathbf{C_1} = \mathbf{A_n}$). Moreover, we denote

$$\breve{\mathbf{N}} = \prod_{j=n-1}^{0} \mathbf{N_j}$$

and

$$\breve{\mathbf{T}} = \sum_{\mathbf{j=0}}^{\mathbf{n-1}} \left(\left(\prod_{\mathbf{k=n-1}}^{\mathbf{j}} \mathbf{N_k}\right) \mathbf{N_j^{-1} T_j} \left(\mathbf{N_j^T}\right)^{-1} \left(\prod_{\mathbf{k=j}}^{\mathbf{n-1}} \mathbf{N_k^T}\right)\right) \tag{12}$$

and rewrite equation (11) as

$$\mathbf{C_{i+1}} = \breve{\mathbf{N}} \mathbf{C_i} \breve{\mathbf{N}}^{\mathbf{T}} + \breve{\mathbf{T}}. \tag{13}$$

By proving, that $\mathbf{C_i}$ converges to a finite matrix as i grows to infinity, we prove Theorem 1.

3.6 Convergence conditions

Expression (13) is the Lyapunov discrete equation (Lyapunov, 1992). If all eigenvalues of $\mathbf{\breve{N}}$ lie within a unit circle and $\mathbf{\breve{T}}$ is symmetric then $\lim_{i\to\infty}\mathbf{C_i}$ is finite and equal to $\mathbf{C}_\infty$, which can be obtained by solution of the algebraic equation

$$\mathbf{C}_\infty = \mathbf{\breve{N}}\mathbf{C}_\infty\mathbf{\breve{N}^T} + \mathbf{\breve{T}}. \tag{14}$$

Since the matrix $\mathbf{S_i}$ is symmetric, $\mathbf{T_i} = \mathbf{R_i^T S_i R_i}$ is also symmetric. The product $\mathbf{XT_iX^T}$ is symmetric for any $\mathbf{X}$ and therefore all addends in (12) are symmetric. Addition preserves symmetry and therefore the matrix

$$\mathbf{\breve{T}} = \sum_{\mathbf{j=0}}^{\mathbf{n-1}}\left(\left(\prod_{\mathbf{k=n-1}}^{\mathbf{j}}\mathbf{N_k}\right)\mathbf{N_j^{-1}T_j}\left(\mathbf{N_j^T}\right)^{\mathbf{-1}}\left(\prod_{\mathbf{k=j}}^{\mathbf{n-1}}\mathbf{N_k^T}\right)\right)$$

is symmetric.

To prove that the eigenvalues of $\mathbf{\breve{N}}$ lie within a unit circle, we exploit positiveness of the matrices $\mathbf{M_i}$ and $\mathbf{R_i}$. Since $\mathbf{M_i}$ is positive, $\mathbf{N_i} = \mathbf{R_i^T M_i R_i}$ is also positive. Moreover, as every $\mathbf{N_i}$ equals to $\mathbf{R_i^T M_i R_i}$, its eigenvalues are the same as those of $\mathbf{M_i}$ and eigenvectors are columns of $\mathbf{R_i}$. The eigenvalues of $\mathbf{N_i}$ therefore correspond to one and $e^{-\frac{s_i}{\rho_i}}$. Since the product $\mathbf{XY}$ of a positive definite matrix $\mathbf{X}$ and a symmetric positive definite matrix $\mathbf{Y}$ is positive definite, the matrix $\mathbf{\breve{N}}$ is positive definite as well. Moreover, the dominant (maximal) eigenvalue of the product $\mathbf{XY}$ is lower or equal than xy, where x and y are dominant eigenvalues of $\mathbf{X}$ and $\mathbf{Y}$. Since the dominant eigenvalue of every $\mathbf{N_i}$ is one, all eigenvalues of $\mathbf{\breve{N}}$ are smaller or equal to one. The dominant eigenvalue of $\mathbf{\breve{N}}$ is equal to one if and only if the dominant eigenvalue of the product $\mathbf{N_{i+1}N_i}$ equals to 1 for all i. Conditions satisfying that the eigenvalues of a product $\mathbf{N_{i+1}N_i}$ are lower than one ensure existence of a finite solution of equation (14). Therefore, we have to find those conditions to support the closed path stability property.

3.7 Convergence proof

We will exploit the fact that a product of matrix eigenvalues equals the matrix determinant and the sum of eigenvalues equals matrix trace. Let us denote eigenvalues of the matrix product $\mathbf{N_{i+1}N_i}$ as $\lambda_{0,1}$ and the smaller eigenvalue of $\mathbf{N_i}$ as n_i ($n_i = e^{-\frac{s_i}{\rho_i}}$). For our convenience, we denote $j = i + 1$. Therefore

$$\det\left(\mathbf{N_j N_i}\right) = \det\mathbf{N_j}\det\mathbf{N_i} = \lambda_0\lambda_1 = n_i n_j \tag{15}$$

If $\lambda_{0,1} \in \langle 0, 1\rangle$, we can state that

$$(1-\lambda_0)(1-\lambda_1) \geq 0, \tag{16}$$

and therefore

$$\lambda_0\lambda_1 - \lambda_0 - \lambda_1 + 1 \geq 0. \tag{17}$$

Combining (15) and (17) we obtain

$$1 + n_i n_j \geq \lambda_0 + \lambda_1.$$

Considering that the sum of eigenvalues equals matrix trace, we get

$$trace\left(\mathbf{R_j^T M_j R_j R_i^T M_i R_i}\right) \leq 1 + n_i n_j. \tag{18}$$

Since $trace(\mathbf{AB})$ is equal to $trace(\mathbf{BA})$, we can rewrite (18) as

$$trace\left(\mathbf{M_j}(\mathbf{R_i R_j^T})^{\mathbf{T}}\mathbf{M_i R_i R_j^T}\right) \leq 1 + n_i n_j. \tag{19}$$

Both matrices $\mathbf{R_i}$ and $\mathbf{R_j}$ represent rotations. The matrix $\mathbf{R_i}$ denotes rotation by the angle α_i and $\mathbf{R_j}$ denotes rotation by the angle α_j. Their product $\mathbf{R_i}\mathbf{R_j^T}$ denotes rotation by $\alpha_i - \alpha_j$. If we denote $\beta = \alpha_i - \alpha_j$ and $\mathbf{R}_\beta = \mathbf{R_i}\mathbf{R_j^T}$, equation (19) is changed to

$$trace\left(\mathbf{M_j}\mathbf{R}_\beta^\mathbf{T}\mathbf{M_i}\mathbf{R}_\beta\right) \leq 1 + n_i n_j. \tag{20}$$

By expanding matrices $\mathbf{M_j}\mathbf{R}_\beta^\mathbf{T}$, we obtain

$$\mathbf{M_j}\mathbf{R}_\beta^\mathbf{T} = \begin{pmatrix} \cos\beta & -n_j\sin\beta \\ \sin\beta & n_j\cos\beta \end{pmatrix},$$

and

$$\mathbf{M_i}\mathbf{R}_\beta = \begin{pmatrix} \cos\beta & n_i\sin\beta \\ -\sin\beta & n_i\cos\beta \end{pmatrix}.$$

Inequality (20) can be rewritten to

$$(1 + n_i n_j)\cos^2\beta + (n_i + n_j)\sin^2\beta \leq 1 + n_i n_j,$$

and further reduced to

$$1 + n_i n_j - (1 - n_i - n_j + n_i n_j)\sin^2\beta \leq 1 + n_i n_j.$$

Finally, we get

$$(1 - n_i)(1 - n_j)\sin^2\beta \geq 0. \tag{21}$$

Since $n_i = e^{-\frac{s_i}{\rho_i}}$, $n_i \in (0,1)$ and $n_j \in (0,1)$, and inequality (21) is strict for $\sin\beta \neq 0$. This fact implies that inequality (16) is strict as well, which means that both λ_0 and λ_1 are lower than one. Therefore both eigenvalues of the matrix product $(\mathbf{N_i}\mathbf{N_j})$ are smaller than one if $\beta \neq n\pi | n \in \mathcal{N}$. The matrix $\breve{\mathbf{N}}$ has both eigenvalues smaller than one if and only if at least two conjoined segments of the path form an angle different from 0 or π.

Since all eigenvalues of $\breve{\mathbf{N}}$ lie within a unit circle and $\breve{\mathbf{T}}$ is symmetric, the covariance matrix $\mathbf{C}_\infty$ denoting the robot position uncertainty at the start of the first path segment is finite and obtainable by a solution of the algebraic equation

$$\mathbf{C}_\infty = \breve{\mathbf{N}}\mathbf{C}_\infty\breve{\mathbf{N}}^\mathbf{T} + \breve{\mathbf{T}}.$$

□

3.8 Convergence proof overview

We have established equations (7) describing the movement of a robot using a navigation method, which is described in Section 2. Equation (10) allowed us to examine the robot position uncertainty evolution as it travels through a known environment. Modifying (10) to closed trajectories, we could rewrite it as (13). By examining conditions, under which (13) has a finite solution, we have proven Theorem 1 for closed paths, which have at least two non-collinear segments. Existence of a finite solution of equation (13) means that if a mobile robot traverses repeatedly a closed polygonal path using our method, its position error at every point of the traversed trajectory will stabilize at a certain value.

4 Practical Issues

The theoretical proof of convergence stands on several assumptions, which might not be always met. In this section, we will outline possible issues, which might arise from incorrect assumptions and discuss their impact on the navigation stability and accuracy. Moreover, we will discuss method requirements in terms of computational power, memory and disk storage.

4.1 Convergence Proof from an Engineer's Point of View

Though elegant and useful, mathematical models and formal proofs are often based on a simplification of reality. A good mathematical model picks out the essence of the modeled problem and concentrates on the examination of the model properties. Some properties of the real system are not included in the model and therefore are not considered. An experienced engineer must be aware of these properties and realize the difference between math and reality. This applies to the proof presented in the Section 3 as well.

In practice, extremely elongated (imagine a rectangle with sides 1000 m and 0.001 m long) paths will not retain the closed path stability property because the movement along the shorter side will not compensate odometry errors accumulated over the long side. Moreover, the model does not cover the probability that the robot will not establish enough correct correspondences because its position error would grow too high. This might easily happen in the case the robot has to avoid large obstacles as well as for paths with very long segments.

Moreover, the fact that the position error does not diverge might not be really useful in real robotic systems. In practice, the real precision is more important. The precision can be estimated using equation (13) if the learned path shape, landmark distribution ρ, camera noise τ and odometry noise ϵ are known. Using $\rho = 20$ (i.e. most of the sensed landmarks are 20 meters in front of the robot), the sensor noise $\tau = 0.1$ and the odometry noise $\epsilon = 0.0005$ for a square, one kilometer long path, the predicted navigation repeatability (i.e. computed from eigenvalues of $\mathbf{C}_\infty$) is 0.15 m. This value is in good accordance with the experimental results presented in Section 5, where the measured repeatability in an outdoor scenarios was 0.14 m.

4.2 Reliance on Odometry

An odometry is regarded as unsuitable for long-term localization due to cumulative errors. Its error model is usually multiplicative with the precision around 1%. The error of the odometric pose estimation is caused mainly by the fact that the robot heading cannot be properly determined. On the other side, odometry can be very precise for traveled distance measurements. Moreover, an odometric error is usually systematic, which can be solved by precise calibration. Our experience with the P3AT robot shows that repeatability of its odometric measurements of the traveled distance on paved roads is better than 0.1%. This means, that in the case of precise heading estimation, the robot would be able to travel 1 km with the position error lower that 1 m.

Our approach relies on the fact that the robot changes direction often enough. If the robot would travel in a straight direction for a long distance, its position error might grow beyond acceptable level. This might be avoided either by forcing the robot to change directions during the learning phase or by complementing the distance measurement by methods without a long-term drift. An example of such a method might be GPS or a vision-based localization used in methods (Royer et al., 2007; Zhang and Kleeman, 2009; Chen and Birchfield, 2009).

4.3 False Correspondences

The most troublesome issue is that correct correspondences might not be established. However, our algorithm works even in cases of a large number of outliers. Consider a situation in which the system is navigating and all of its established correspondences are false. The horizontal position deviation of detected and mapped features would be basically a random variable. Therefore a histogram H, which is built in order to establish the robot turning speed, will have its bins (approximately) equally filled. The robot turning speed will therefore be random. Now consider, that there are a few correctly established correspondences. Each correctly established correspondence increases the value of the bin, which corresponds to the robot's true heading deviation. Therefore the probability that the correct bin has a maximal value increases with each correct correspondence.

This is different from the work presented in (Chen and Birchfield, 2009; Segvic et al., 2007), where the authors choose a mean of horizontal differences instead of the modus. The modus is more invariant to the incorrect correspondences than the mean, which makes our method more precise and robust.

In reality, we get 80%-90% correctly established correspondences if the navigation phase follows mapping immediately. As the map gets older, the ratio of correct correspondences tends to drop. The rate of "map decay" depends on the environment and is caused mainly by two factors: short-term lighting changes caused by a change in position of the Sun and the current weather conditions and long-term environment changes caused by seasonal factors. Both illumination and long-term changes are not so significant in indoor environments, because lighting is typically artificial and the seasonal changes do not happen. So it is expected, that illuminations and seasonal changes would play an important role in outdoor environments.

To evaluate the system robustness to lighting changes, we have made an all-day experiment, in which the robot traversed 1 km long path in an outdoor environment, see Section 5.5. To evaluate our system robustness to seasonal environment changes, we have mapped a 50 m long path in a park. The path has been autonomously navigated and then re-learned one month later. This has been done in five consecutive months, see Section 5.4. The results of both experiments show that the system is robust to both long-term and short-term environment changes.

Dynamic objects and occlusions cause only a temporary and slight decrease of the ratio of correctly established correspondences. During the experiments, we did not notice any problems with moving objects in the robot field of view.

4.4 Obstacle avoidance

The proposed navigation method itself does not include obstacle avoidance. However, it can be complemented by a collision avoidance module, which takes control of the robot whenever an obstacle in the robot's course is detected. Such a module guides the robot around the obstacle until the area between the robot and its path is clear again. After that, the visual-based navigation takes control and guides the robot by Algorithm 2.

Since obstacles have finite dimensions, the robot position error will grow by a finite value every time it passes an obstacle. From the theoretical point of view, random obstacles in the robot path can be modeled by the addition of a random vector with a zero mean to $\mathbf{s}$ in equation (8). Although the addition will increase the matrix $\mathbf{S}$ in equation (9), the symmetry of $\mathbf{S}$ will be preserved. Obstacles would therefore increase the matrix $\breve{\mathbf{T}}$ in equations (13,14), but since $\breve{\mathbf{T}}$ remains symmetric, equation (14) will have a unique solution. However, the robot position uncertainty, represented by the matrix $\mathbf{C}_\infty$, will increase. Therefore, obstacle avoidance would decrease precision of the robot navigation, but it should remain stable. This assumption is experimentally verified in Section 5.3.

It‘s clear that there exists a size of obstacles for which the algorithm will fail, because after circumnavigating the obstacle, the robot will not find previously mapped features.

4.5 Systematic errors

Since the navigation algorithm relies on two sensors, there are two sources of systematic errors in our algorithm: the odometry and the camera.

The systematic error of the odometry means that if the robot will traverse the distance d, it will report that the traveled distance is $d(1+\eta)$. Let us consider that the robot has 900% odometric error, i.e. $\eta = 9$. During mapping phases, the error will cause the segment lengths s and landmark data f and g to be 10 times higher in the map than in reality. However, in the navigation phases, the odometry error will give 10 times higher values of the robot distance from the segment start and therefore errors in the map and robot position error will suppress each other.

The systematic error of the camera might be caused by the misalignment of the camera optical axis and the robot body. This causes the positions of landmarks $\mathbf{u}$, $\mathbf{v}$ in the map to be different from a case with an ideal camera. However, when the robot encounters the same location, detected landmark positions will be shifted the same way as in the learning phase. The systematic error will therefore cancel out as in the previous case.

A different case would be a change of the odometric error η or the camera angle θ between the learning and navigation phases. From a theoretical point of view, this would cause a change of the vector $\mathbf{s}$. Unlike in the previous case, the vector $\mathbf{s}$ will not be modified by a random vector, but a fixed one. It means that $\tilde{\mathbf{s}}$ will remain the same and matrix $\breve{\mathbf{T}}$ will preserve symmetricity. Systematic errors would cause the robot to traverse a trajectory slightly different from the learned one, but should not affect navigation stability. However, the algorithm will fail to establish correct correspondences between the mapped and detected features if the systematic errors are too high.

The experimental evaluation of the influence of systematic errors on the navigation stability is described in Section 5.2. Even though the systematic errors have been set to high values during the experimental evaluation, the navigation stability has been preserved.

4.6 Necessity of a compass

Relying on a compass only for heading estimation has shown to be a weakpoint during experiments performed in year 2008 and 2009. During learning phases, the compass noise caused an incorrect azimuth estimation of some segments.

Therefore, we considered replacing the absolute azimuth measurements by relative ones. So, instead of recording α_i for i^{th} segment in the learning phase, the azimuth relative to the previous segment (i.e. $\Delta_i = \alpha_i - \alpha_{i-1}$) is recorded in the map. The relative azimuth Δ_i can be estimated either by the odometry or by the tracking of the features during transitions to the next segment. This approach is applicable in cases, where a robot is taught a path, which is supposed to be traversed later. However, sometimes it is necessary to create a more complex, graph-like map, see Section 5.7.

In more complex cases, the robot creates a map of the large environment in several mapping runs, and traverses the given sequence of segments in a different order than in the mapped sequence. In this case, sole knowledge of the relative segment azimuths is not sufficient, because angles between nonconsecutive segments are not known to us. Of course an angle between i^{th} and $(i+j)^{th}$ segment can be estimated by summing all relative angles between segments i and $i+j$, but since every Δ_i contains a small error, the error of the sum is too large for long j.

To deal with these more complex cases, we have implemented a simple Kalman filter, which fuses data from odometry and compass. The filter suppresses the compass noise and causes the absolute heading measurements to be more reliable. However, the filter was implemented at the end of 2009, so in the previous experiments the compass noise caused trouble.

4.7 Computational and Storage Requirements

To estimate computational and storage requirements, we have used data from the experiment described in Section 5.5.

We evaluated the computational requirements in terms of required computational time spent in various stages of the algorithm. The most computationally intensive stage of the algorithm is the feature extraction, which takes 260 ms on average. About 30 ms is taken by establishing proper correspondences. The histogram voting time is lower than 1 ms. During experiments, the camera image and additional parameters of the algorithm were displayed for debugging purposes. Drawing these data on a computer screen takes about 60 ms. Thus, the entire control loop takes about 350 ms.

The average landmark density is about 140 landmarks per meter of the path. The map is stored on the hard drive in a text format, see Table 1, and one landmark occupies about 800 bytes. Therefore, the disk storage needed for one kilometer of path is about 112 MB. Once loaded to the computer memory, a landmark is represented in binary and occupies less than 300 bytes. Thus, a segment 1 km long would take 42 MB of computer memory.

5 Experiments

The assumptions formed in Sections 3 and 4 have been verified in several real-world experiments. The experimental evaluation has been performed in seven different scenarios examining:

1. convergence for two types of paths - with and without the closed path stability property,
2. the impact of systematic errors to the navigation precision,
3. feasibility of complementing the method by the collision avoidance module,
4. robustness to environment changes and variable lighting conditions,
5. performance in environments with landmark deficiency,
6. navigation efficiency for long paths in an outdoor environment with diverse terrain,
7. real deployment of the navigation procedure in RoboTour 2008 and RoboTour 2009 contests (Iša and Dlouhý, 2010).

During these scenarios, the robot has autonomously traversed over 3 km of indoor and over 25 km of outdoor paths. The P3AT platform with the configuration described in Section 2 was used in all testing scenarios.

The robot has learned different closed paths and has been requested to navigate these paths several times, in the first six scenarios. The relative position $\mathbf{c_i}$ of the robot to the path start was measured every time the robot completed the i-th path loop. To evaluate the quality of the navigation algorithm, accuracy and repeatability values like in (Chen and Birchfield, 2009) have been used. The accuracy ε_{acc} and the repeatability ε_{rep} is computed as the RMS of the Euclidean distance or the standard deviation of robot's final positions from the path start

$$\varepsilon_{acc} = \sqrt{\tfrac{1}{n-j}\sum_{i=j}^{n} \|\mathbf{c_i}\|^2} \qquad \varepsilon_{rep} = \sqrt{\tfrac{1}{n-j}\sum_{i=j}^{n} \|\mathbf{c_i}-\mu\|^2}, \tag{22}$$

where $\mathbf{c_i}$ is the robot position relative to the path start after completing the i-th loop and $\mu = \sum_{i=j}^{n} \mathbf{c_i}/(n-j)$. In most scenarios, the initial robot position was intentionally changed to be 1.5 m apart from the learned path start. In these cases, we do not set j to 1, but wait five loops until the initial position error diminishes. Thus, the repeatability and the accuracy is computed for $j = 5$, $n = 20$ in the first four scenarios.

5.1 Stability of Robot Position for Different Types of Paths

The scenario examines Theorem 1 for paths with and without the closed path stability property. The conclusions made in Section 3 indicate that paths with all collinear segments do not retain the closed path stability property, while other paths do. The following paths have been considered: a path with only two collinear segments (i.e. "back and forth" line path) and a square path. At first, the robot has been taught these closed paths in an indoor hall. After that, the robot has been placed either directly at the path start or 1.5 m away and requested to navigate along the learned path for twenty times. The robot position $\mathbf{c_i}$ has been measured after each completed loop.

The first (degenerate) path has been formed of two collinear, five meter long, segments. The square path has been composed of four segments, each five meters long, with the end of the last segment identical to the segment at the start of the path. The distance of the robot from the path start after each loop (i.e. $\|\mathbf{c_i}\|$) is shown in Figure 4.

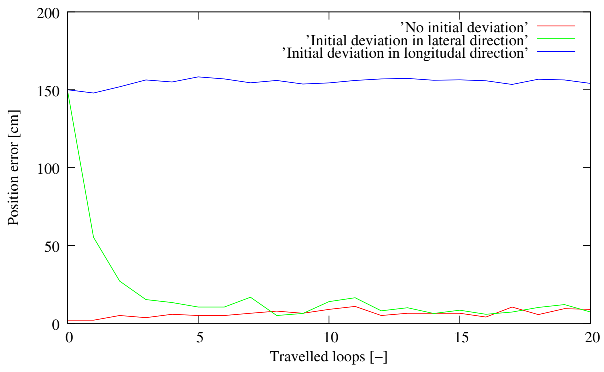

(a) The position error for line (degenerate) path.

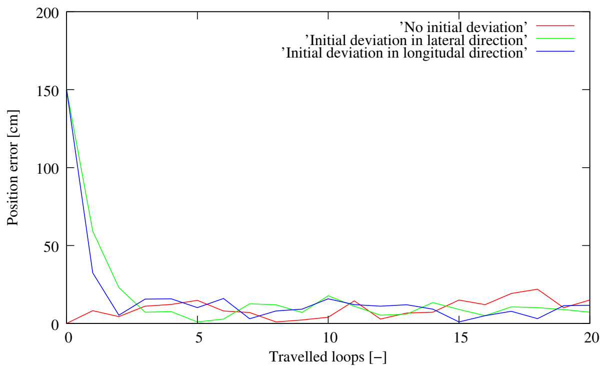

(b) The position error for square (normal) path.

Figure 4: The position error for paths without and with the stability property.

The values indicate that for square trajectories, the robot has been able to correct the position error that has been introduced at the beginning of navigation along the learned path. Only the error in y-coordinate (i.e. coordinate axis normal to path segments) has been partially corrected for collinear trajectories, while the x-coordinate stayed uncorrected. These experimental results confirm the theoretical assumptions described in Section 3.8, stating that the navigation is unstable for paths with only collinear segments.

The robot has traversed over 1.8 km in this scenario. Both the accuracy and the repeatability for the twenty meter long square paths were 0.10 m.

5.2 Effect of Systematic Errors

The effect of the systematic errors to the navigation precision has been evaluated in this scenario. Two sources of systematic errors have been considered: the camera and the odometry. An error of the camera can be caused by its optical axis deviation and the odometric error can be caused by a tire pressure change. To show the effect of the parameters change, it is necessary to modify these parameters between the learning and the navigation phases, otherwise a path is learned with the systematic errors and therefore the errors do not have effect.

The following experiments have been performed to verify that small scale systematic errors do not affect the navigation stability. At first, the robot camera has been panned by 10° and the robot has been requested to traverse the square path learned during the scenario 5.1 twenty times. Then, a 10% systematic odometry error has been introduced[1]. Finally, the robot has been requested to traverse the path twenty times with both 10% odometry and 10° camera bias. As in the previous cases, the robot position $\mathbf{c_i}$ has been measured each time the robot reached the learned path start. The measured distances from the path start are shown in Figure 5.

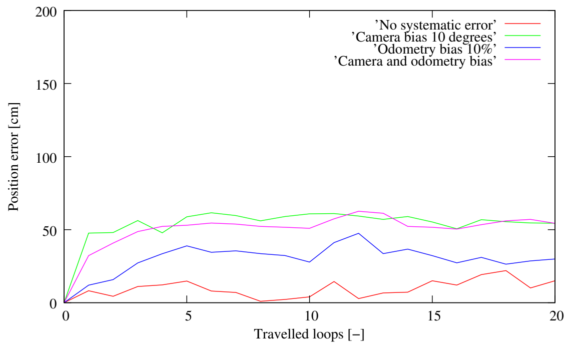

Figure 5: Systematic errors effect: The position error for different types of systematic errors.

The results show that the odometric and the camera biases cause errors in robot positioning, but the error does not diverge. After a few loops, the position error does not grow any more and the system reaches a steady state. The overall accuracy is lower than without the systematic errors, but repeatability remains similar to the previous scenarios.

The robot has traversed over 1.2 km in this scenario. The average accuracy with the camera bias has been 0.58 m and the odometry bias has caused accuracy to change to 0.34 m. When both the odometry and the camera were biased, the accuracy has been 0.55 m. The average repeatability has been lower than in the previous scenario, i.e. 0.06 m.

5.3 Obstacle Avoidance

A simple collision avoidance module (based on the robot sonars) has been activated in this scenario. The collision avoidance is based on the Tangent Bug algorithm with a finite range sensor (Choset et al., 2005). When the robot detects an obstacle on its course, the visual based navigation is suppressed and the robot starts to circumnavigate the detected obstacle. During the circumnavigation, the odometry is used to determine the robot position and the sonar data is used to estimate the obstacle position. The visual navigation algorithm is resumed when the path between the robot and the end of the current segment is clear.

The robot was taught a square path similar to the one used in scenario 5.1. After that, one obstacle[2] on each path segment has been placed and the robot navigated the path twenty times.

The robot autonomously navigated approximately 0.4 km with the accuracy of 0.16 m and the repeatability of 0.08 m. It is clear that the position precision was affected, but did not diverge.

[1]This has been done in software - a distance of the robot from the segment start measured by the odometry has been multiplied by the factor of 1.1 before it was passed to the navigation algorithm.

[2]Obstacle dimensions were approximately a half of the robot size.

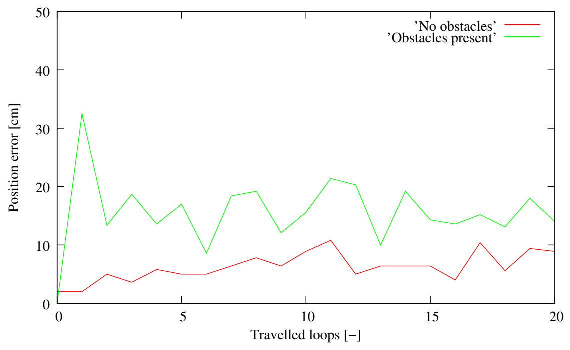

Figure 6: Obstacle avoidance experiment: The position errors with and without obstacles.

5.4 Environment and Lighting Changes

The effect of variable lighting conditions and the long-term environment changes have been examined in this scenario. At first, the robot has been taught a closed, 50 m long path consisting of five segments in the Stromovka park located in the city of Prague. One month later, the robot has been placed 1.5 m away from the path start and has been requested to navigate the path twenty times. This procedure has been repeated five times, i.e. the test has been done every month from November 2009 till April 2010. In each experiment, the robot used a map created in a previous month. The measured distances are shown in Figure 7.

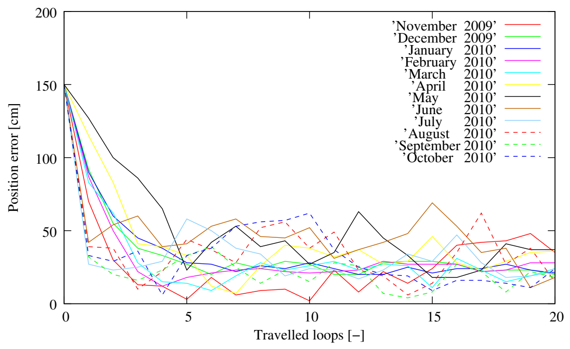

Figure 7: The position errors on different months of the long-term experiment.

Not only the lighting conditions differed every time but also the environment went through seasonal changes. To document these changes, a picture from the on-board camera has been stored every time the mapping has been initiated, see Figure 8. There were considerably less correct correspondences between recognized and learned features. With a map created just before the navigation, the robot usually correctly recognizes 70-90% of learned landmarks. Using one month old map, the ratio of the correctly recognized landmarks drops to 10-40%. Nevertheless the robot was able to correct its initial position error and was able to traverse the path faultlessly in all cases.

The robot autonomously navigated over 6 km with an average accuracy of 0.24 m in this scenario. Unlike in previous scenarios, we did not measure the robot position $\mathbf{c_i}$ after completion of each loop, but we only recorded the robot distance from the path start, i.e. $\|\mathbf{c_i}\|$. Therefore, the repeatability cannot be calculated by equations (22). Except for winter months, pedestrians regularly crossed the robot path and moved in the robot's field of view.

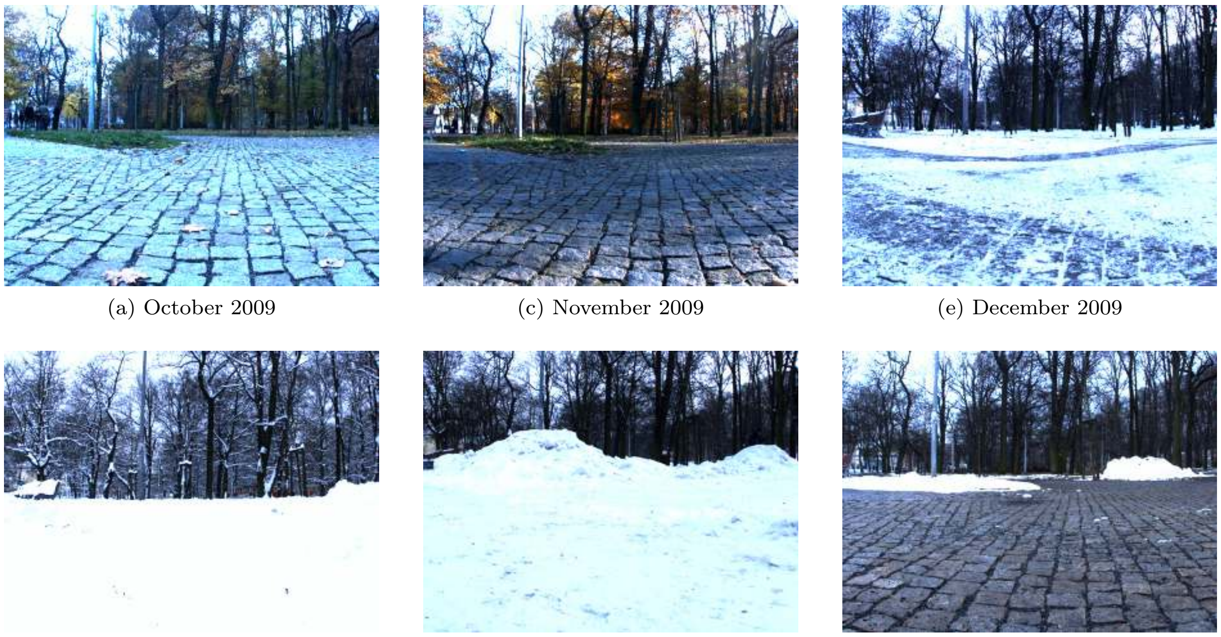

(a) October 2009 (c) November 2009 (e) December 2009

(b) January 2010 (d) February 2010 (f) March 2010

Figure 8: Long-term experiment: The view from the robot's camera at the path start in different months.

5.5 One-day Outdoor Experiment

The system performance for long paths has been evaluated in a realistic outdoor environment. The experiment was performed around the Proboštov pond[3] in Proboštov, Czech republic at the end of March 2010.

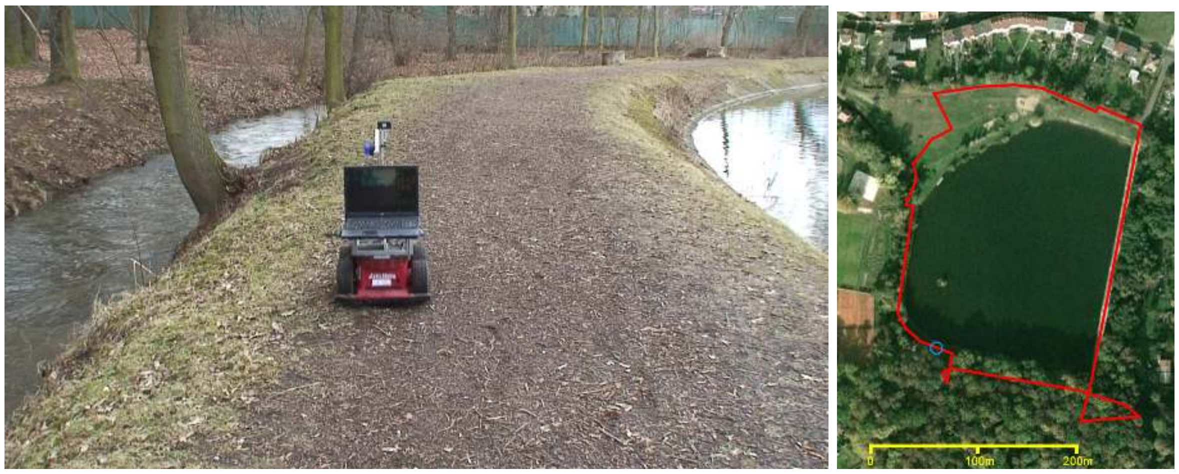

Figure 9: One-day experiment: The path around Proboštov pond and the dirt road terrain example.

The robot has been taught a 1 km long path around the pond in the morning. The path went through a variable non-flat terrain with asphalt paths, dirt roads, footpaths and grass terrain in an approximately equal ratio. After the path has been taught, the robot has been placed 1.5 m away from the path start and requested to traverse it repeatedly. Every time it reached the path start, its position was measured and its

[3]Proboštov pond 50°39'58.716"N, 13°50'18.35"E

batteries replaced (the robot was not moved during the battery exchange). It took approximately one hour for the robot to traverse the learned path and the battery replacement took fifteen minutes. The weather changed from cloudy/light rain to partly cloudy/sunny during the experiment. In the afternoon, a lot of pedestrians showed up and have either entered robot's field of view or crossed its path.

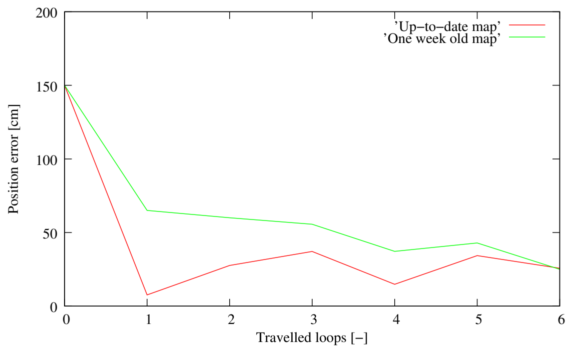

Figure 10: The position errors of the one-day experiment.

Nevertheless, the robot has been able to complete the learned path six times before nightfall. The robot has traversed 6 km with the accuracy[4] of 0.26 m and the repeatability of 0.14 m. The experiment was repeated (without the learning phase) one week later and the robot traversed the path six times with the accuracy of 0.31 m and repeatability of 0.20 m.

5.6 Landmark deficiency experiment

We have claimed that the system is able to operate in an environment, which contains a low number of landmarks. To verify this assumption, we have taught the robot an outdoor path during night and let it navigate using only streetlamp lights. The robot has been taught a 0.3 km long path on paved roads in a residential area. The on-board camera iris has been fully opened and the camera exposure time has been set to 0.37 s. The path has been taught at midnight so more than 90% of the mapped landmarks were streetlamps and illuminated windows.

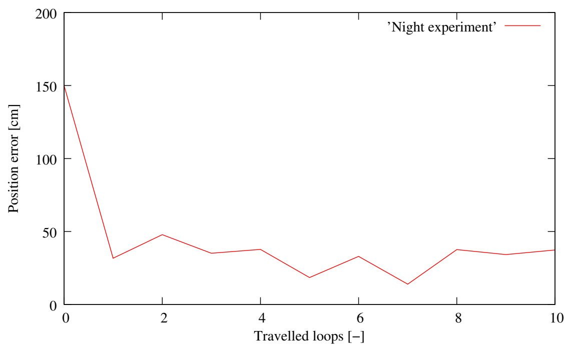

Figure 11: The position errors of the landmark deficiency (night) experiment.

After the path has been learned, the robot has been placed 1.5 m away from the path start and requested to traverse it ten times. On the contrary to day experiments, in which the robot detected typically 150-300 landmarks, during night, the typical number of landmarks was three. The robot has traversed 3 km with the accuracy[5] of 0.32 m and the repeatability of 0.16 m.

[4]In this case, ε_{acc} and ε_{rep} were computed with $j = 3$ and $n = 6$ in equations (22)

[5]In this case, ε_{acc} and ε_{rep} were computed with $j = 3$ and $n = 10$ in equations (22)

5.7 The RoboTour Outdoor Delivery Challenge

The RoboTour contest (Iša and Dlouhý, 2010; Dlouhy and Winkler, 2009) is an international autonomous robot delivery challenge organized by `robotika.cz`. The participating teams are mostly from Czech and Slovak universities. The competition is a perfect event for an independent verification of the system functions and comparison with other navigation methods. However, not only the navigation methods are evaluated, but also the complete systems including all hardware parts are tested.

Fully autonomous robots have to travel a random path in a park, stay on the pavements and detect randomly placed obstacles in this challenge. A map of the park with its pathways (designated by letters) is given to the teams in advance. The competition consists of several rounds, each with a different path. Thirty minutes before each round, referees choose a random closed path and announce it as a sequence of letters. Competing teams place their robots at the starting positions and execute their autonomous navigation algorithms. Robots must travel without leaving the pathway and without colliding with any random obstacles. The robot score is determined according to its traveled distance. In 2008, the competition was held in Stromovka park[6] in Prague, Czech republic. One year later, the contest moved to park Lužánky[7] in Brno, Czech republic.

The Stromovka park pathways have been mapped two days prior to the competition. The competition had five rounds with different pathways, see Table 2. The robot completed the required path four times, out of these five attempts. During two of these attempts, the robot did not leave the pathway at all and during two others, the robot had partially left (i.e. with two side wheels) the pathway. In cases when the robot has left the pathway partially, it was left to continue moving (without additional scores) and reached the goal area. One failed attempt was caused by a battery failure.

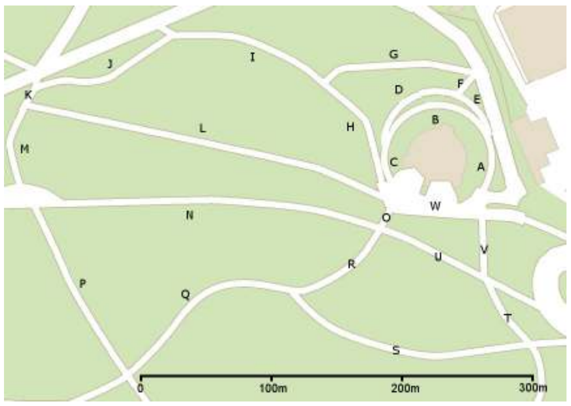

(a) RoboTour 2008

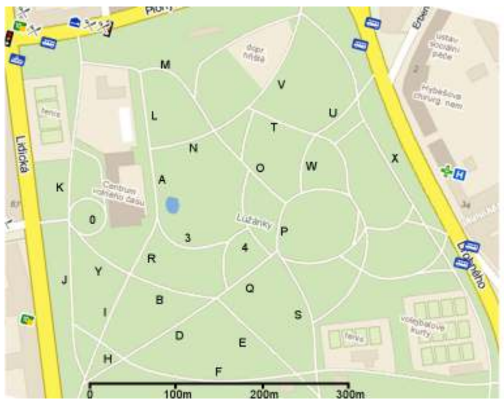

(b) RoboTour 2009

Figure 12: RoboTour 2008/2009 pathway maps

The competition in Lužánky park was performed in a larger part of the environment, hence the mapping took three days. The total length of the mapped pathways was 8 km, the map consisted of approximately one million landmarks, which took 834 MB of disk space. The competition had four rounds, see Table 2. The robot was able to complete the required paths two times. One attempt failed due to wrong compass reading during the path learning, but after a manual correction of the robot heading, the robot caught up and reached the goal area. The other failed attempt was caused by a human factor.

Although the performance has not been perfect, the robot was able to travel the required trajectory and our

[6]Kralovska obora aka Stromovka 50°6'18.778"N, 14°25'33.395"E
[7]Lužánky park 49°12'25.516"N, 16°36'29.81"E

Table 2: RoboTour 2008 and 2009 paths

(a) RoboTour 2008

Pathway sequence	**Length** [m]
ABCW	250
ORQPMKJIH	850
ABCHGFDCW	500
HGFEAWOUVW	600
UTSROCDEBCW	700
Total	2 900

(b) RoboTour 2009

Pathway sequence	**Length** [m]
ALK0JIR	800
BESQDGHJ0Y	1050
34PWTMLA	750
0YR34SFHJ	600
Total	2 200

team has reached the first rank for both events in 2008 and 2009.

5.8 Experiment Summary

The results of the aforementioned experiments confirm not only theoretical assumptions stated in Section 3, but they also show that our method is feasible for use in real-world conditions. The proposed method is able to cope with diverse terrain, dynamic objects, obstacles, systematic errors, variable lighting conditions and seasonal environment changes. The summary of experiments in Table 3 indicates, that the localization precision of our method is slightly worse than in closely related methods presented in (Royer et al., 2007; Zhang and Kleeman, 2009). Lower precision is probably caused by heavy reliance on odometry and suboptimal use of visual information.

Table 3: Proposed method accuracy and repeatability in various scenarios

		Indoor clear	**Indoor obstacles**	**Outdoor long-term**	**Outdoor one-day**	**Outdoor night**
Accuracy	[m]	0.10	0.16	0.24	0.25	0.32
Repeatability	[m]	0.10	0.08	N/A	0.14	0.16
Loop length	[m]	20	20	50	1040	330

Compared to the similar method presented in (Chen and Birchfield, 2009), our method accuracy and repeatability is better in outdoor environments. A probable reason of this is that we used a modus to determine robot heading. The authors of (Chen and Birchfield, 2009) use a mean of horizontal deviations, which is less robust to data association errors.

6 Conclusion

A simple navigation method based on bearing-only sensors and an odometry was presented. In this method, a robot navigating known environment uses a map of the environment and a camera input to establish its heading, while measuring the traveled distance by the odometry. We claim that this kind of navigation is sufficient to keep the robot position error limited. This claim is formulated as a closed path stability property and proved for polygonal paths with at least two non-collinear segments. The property allows to estimate the robot position uncertainty based on the landmark density, robot odometry precision and path shape.

The proposed method has been experimentally verified by a mobile robot with a monocular camera. The robot builds a SURF-based (Bay et al., 2006; Cornelis and Gool, 2008) landmark map in a guided tour. After that, it uses the aforementioned method to autonomously navigate in the mapped environment.

We have conducted experiments indicating that theoretical results and assumed conditions are sound.

The proposed navigation method has surprising properties different from the properties of other navigation and localization methods, mainly

- the robot can perform 2D localization by heading estimation, which is 1-DOF method,
- if the robot travels between two points, it is better to use a "zig-zag" trajectory rather than a straight one,
- traveling a closed trajectory might reduce the robot position uncertainty.

We believe, that the convergence proof does not apply to our system only, but is valid for many other algorithms. The proof suggests that any algorithm, which decreases the lateral position error of a robot, is stable for closed polygonal trajectories. This might be the case of even simpler and faster methods, such as the one presented in (Zhang and Kleeman, 2009). However, this is merely a hypothesis, which needs to be thoroughly examined.

The fundamental limitation of our method is its reliance on odometric measurements. Other visual-based navigation methods use the odometry only as an auxiliary measurement or do not require odometry at all. Therefore, these methods would perform better in scenarios, where wheel slippages have to be taken into account. Although our method is limited in application and its precision is lower compared to methods presented in (Zhang and Kleeman, 2009; Royer et al., 2007), we believe that it is interesting from an academical point of view.

In the future, we would like to test our algorithm with robots, which have only imprecise odometry or inaccurate dead-reckoning. The preliminary tests conducted with the AR-Drone quadrotor helicopter, which estimates the traveled distance by accelerometers, seem to be promising.

Acknowledgements

We would like to thank our colleagues for valuable remarks and friends for help with outdoor tests. The work presented in this paper has been supported by the Ministry of Education of the Czech Republic under by the projects MSM 6840770038, 2C06005, by a CTU research grant SGS10/185/OHK3/2T/13 and by the FP7-ICT project "REPLICATOR" No. 216240.

Appendix A: Index to Multimedia Extensions

Index to multimedia extensions

Extension	Media Type	Description
1	Video	Ongoing work.

References

Bay, H., Tuytelaars, T., and Gool, L. (2006). SURF: Speeded up robust features. In *Proceedings of the ninth European Conference on Computer Vision*, Graz, Austria.

Blanc, G., Mezouar, Y., and Martinet, P. (2005). Indoor navigation of a wheeled mobile robot along visual routes. In *Proceedings of International Conference on Robotics and Automation*, Barcelona, Spain.

Bosse, M., Newman, P., Leonard, J. J., and Teller, S. (2004). SLAM in Large-scale Cyclic Environments using the Atlas Framework. *The International Journal of Robotics Research*, 23(12):1113–1139.

Burschka, D. and Hager, G. (2001). Vision-based control of mobile robots. In *Proceedings International Conference on Robotics and Automation*, Seoul, Korea.

Chaumette, F. and Hutchinson, S. (2006). Visual servo control, part I: Basic approaches. *IEEE Robotics and Automation Magazine*, 13(4):82–90.

Chaumette, F. and Hutchinson, S. (2007). Visual servo control, part II: Advanced approaches. *IEEE Robotics and Automation Magazine*, 14(1):109–118.

Chen, Z. and Birchfield, S. T. (2006). Qualitative vision-based mobile robot navigation. In *2006 IEEE International Conference on Robotics and Automation (ICRA)*, IEEE International Conference on Robotics and Automation, pages 2686–2692, Orlando, Florida.

Chen, Z. and Birchfield, S. T. (2009). Qualitative vision-based path following. *IEEE Transactions on Robotics and Automation*, 25(3):749–754.

Choset, H., Lynch, K. M., Hutchinson, S., Kantor, G. A., Burgard, W., Kavraki, L. E., and Thrun, S. (2005). *Principles of Robot Motion: Theory, Algorithms, and Implementations*. MIT Press, Cambridge, MA.

Civera, J., Davison, A. J., and Montiel, J. (2008). Inverse depth parametrization for monocular SLAM. *IEEE Transactions on Robotics*, 24(5):932–945.

Clemente, L. A., Davison, A. J., Reid, I. D., Neira, J., and Tardós, J. D. (2007). Mapping large loops with a single hand-held camera. In Burgard, W., Brock, O., and Stachniss, C., editors, *Robotics: Science and Systems*. The MIT Press.

Cornelis, N. and Gool, L. (2008). Fast scale invariant feature detection and matching on programmable graphics hardware. In *CVPR 2008 Workshop (June 27th)*, Anchorage Alaska.

Davison, A. J., Reid, I. D., Molton, N. D., and Stasse, O. (2007). MonoSLAM: Real-time single camera SLAM. *IEEE Transactions on Pattern Analysis and Machine Intelligence*, 29(6):1052–1067.

DeMenthon, D. and Davis, L. S. (1992). Model-based object pose in 25 lines of code. In *ECCV '92: Proceedings of the Second European Conference on Computer Vision*, Santa Margherita Ligure, Italy.

Dissanayake, M., Newman, P., Clark, S., Durrant-Whyte, H., and Csorba, M. (2001). A solution to the simultaneous localization and map building (SLAM) problem. *IEEE Transactions on robotics and automation*, 17(3):229–241.

Dlouhy, M. and Winkler, Z. (2009). Robotour outdoor delivery challenge. http://robotika.cz/competitions/.

Estrada, C., Neira, J., and Tardós, J. D. (2005). Hierarchical SLAM: real-time accurate mapping of large environments. *IEEE Transactions on Robotics*, 21(4):588–596.

Frese, U. (2006). A discussion of simultaneous localization and mapping. *Autonomous Robots*, 20(1):25–42.

Gibbens, P., Dissanayake, G., and Durrant-Whyte, H. (2000). A closed form solution to the single degree of freedom simultaneous localisation and map building (SLAM) problem. In *Proceedings of the 39th IEEE Conference on Decision and Control*, pages 191–196, Sydney, NSW Australia.

Guerrero, J. J., Martinez-Cantin, R., and Sagüés, C. (2005). Visual map-less navigation based on homographies. *Journal of Robotic Systems*, 22(10):569–581.

Holmes, S., Klein, G., and Murray, D. W. (2008). A Square Root Unscented Kalman Filter for visual monoSLAM. In *2008 IEEE International Conference on Robotics and Automation*, pages 3710–3716, Pasadena, California.

Iša, J. and Dlouhý, M. (2010). Robotour - robotika.cz outdoor delivery challenge. In *Proceedings of the 1-st Slovak-Austrian International Conference on Robotics in Education*, Bratislava, Slovakia. (To appear).

Julier, S. and Uhlmann, J. (2001). A counter example to the theory of simultaneous localization and map building. In *2001 IEEE International Conference on Robotics and Automation*, pages 4238–4243, Seoul, Korea.

Kalman, R. E. (1960). A new approach to linear filtering and prediction problems. *Transactions of the ASME–Journal of Basic Engineering*, 82(Series D):35–45.

Kidono, K., Miura, J., and Shirai, Y. (2000). Autonomous visual navigation of a mobile robot using a human-guided experience. In *Proceedings of 6th Int. Conf. on Intelligent Autonomous Systems*, pages 620–627, Venice, Italy.

Lowe, D. G. (1999). Object recognition from local scale-invariant features. In *ICCV '99: Proceedings of the International Conference on Computer Vision*, page 1150, Kerkyra, Corfu, Greece.

Lowe, D. G. (2004). Distinctive image features from scale-invariant keypoints. *International Journal of Computer Vision*, 60(2):91–110.

Lyapunov, A. (1992). The general problem of stability in motion. *International Journal of Control*, 55(3):531–773.

Martinelli, A., Tomatis, N., and Siegwart, R. (2005). Some results on SLAM and the closing the loop problem. In *International Conference on Intelligent Robots and Systems*, pages 334–339, Edmonton, Canada.

Matsumoto, Y., Inaba, M., and Inoue, H. (1996). Visual navigation using view-sequenced route representation. In *Proceedings of the International Conference on Robotics and Automation*, Minneapolis, USA.

Montiel, J., Civera, J., and Davison, A. (2006). Unified inverse depth parametrization for monocular SLAM. In *Proceedings of Robotics: Science and Systems*, Philadelphia, USA.

Mourikis, A. and Roumeliotis, S. I. (2004). Analysis of positioning uncertainty in simultaneous localization and mapping (SLAM). In *Proceedings of the IEEE/RSJ International Conference on Robotics and Intelligent Systems (IROS)*, Sendai, Japan.

Remazeilles, A. and Chaumette, F. (2007). Image-based robot navigation from an image memory. *Robotics and Autonomous Systems*, 55(4):345–356.

Royer, E., Lhuillier, M., Dhome, M., and Lavest, J.-M. (2007). Monocular vision for mobile robot localization and autonomous navigation. *Internationa Journal of Computer Vision*, 74(3):237–260.

Segvic, S., Remazeilles, A., Diosi, A., and Chaumette, F. (2007). Large scale vision based navigation without an accurate global reconstruction. In *IEEE Int. Conf. on Computer Vision and Pattern Recognition*, Minneapolis, Minnesota, USA.

Segvic, S., Remazeilles, A., Diosi, A., and Chaumette, F. (2009). A mapping and localization framework for scalable appearance-based navigation. *Computer Vision and Image Understanding*, 113(2):172–187.

Svab, J., Krajnik, T., Faigl, J., and Preucil, L. (2009). FPGA-based speeded up robust features. In *2009 IEEE International Conference on Technologies for Practical Robot Applications*, Boston, USA.

Williams, B., Cummins, M., Neira, J., Newman, P., Reid, I., and Tardós, J. (2009). A comparison of loop closing techniques in monocular SLAM. *Robotics and Autonomous Systems*, 57(12):1188–1197.

Wilson, W., Hulls, C., and Bell, G. (1996). Relative end-effector control using cartesian position based visual servoing. *Robotics and Automation*, 12(5):684–696.

Zhang, A. M. and Kleeman, L. (2009). Robust appearance based visual route following for navigation in large-scale outdoor environments. *International Journal of Robotics Research*, 28(3):331–356.

Appendix B

This appendix presents values measured during experiments.

Stability of Robot Position for Different Types of Paths

The table 4 contains data measured during the first experimental scenario presented in Section 5.1. It shows the measured positions for the paths, which do and do not retain the stability property. Note that line (degenerate) paths do not correct the longitudal position deviation, which is in accordance with the convergence proof presented in Section 3.

Table 4: Convergence for degenerate and normal paths - indoor

Loop	**Position relative to start** [m] *line (degenerate) path* $d_{0,0}$	$d_{0,1.5}$	$d_{1.5,0}$	**Position relative to start** [m] *square (normal) path* $d_{0,0}$	$d_{0,1.5}$	$d_{1.5,0}$
00	0.00, 0.00	0.00, 1.50	1.50, 0.00	0.00, 0.00	0.00, 1.50	1.50, 0.00
01	-0.02, 0.00	0.05, 0.55	1.46, -0.24	0.08, -0.02	0.12, 0.58	0.32, -0.06
02	-0.03, -0.04	-0.03, 0.27	1.49, -0.30	0.02, 0.04	0.02, 0.23	0.05, -0.02
03	-0.03, -0.02	-0.06, 0.14	1.53, -0.32	-0.02, 0.11	0.04, 0.06	0.10, 0.12
04	-0.05, 0.03	-0.03, 0.13	1.53, -0.25	0.10, 0.07	-0.07, -0.03	0.05, 0.15
05	-0.05, 0.00	-0.03, 0.10	1.56, -0.27	0.10, 0.11	-0.01, 0.00	0.05, 0.09
06	-0.04, 0.03	-0.03, 0.10	1.55, -0.25	0.08, 0.00	-0.02, 0.02	0.00, -0.16
07	-0.05, 0.04	-0.05, 0.16	1.53, -0.22	0.01, 0.07	0.04, -0.12	-0.03, 0.00
08	-0.05, 0.06	-0.05, 0.00	1.54, -0.25	0.00, -0.01	0.05, 0.11	0.07, 0.04
09	-0.04, 0.05	-0.06, 0.02	1.53, -0.15	-0.01, 0.02	0.05, -0.05	0.07, 0.06
10	-0.04, 0.08	-0.05, 0.13	1.53, -0.21	0.00, -0.04	-0.08, -0.16	0.09, 0.13
11	-0.06, -0.09	-0.04, 0.16	1.54, -0.25	-0.04, -0.14	0.02, -0.11	0.12, 0.02
12	-0.05, 0.01	-0.04, -0.07	1.54, -0.31	0.02, -0.02	0.05, 0.02	0.02, -0.11
13	-0.05, 0.04	-0.08, 0.06	1.55, -0.27	0.03, -0.06	0.00, 0.06	-0.01, -0.12
14	-0.04, 0.05	-0.06, 0.02	1.53, -0.31	0.06, 0.04	-0.09, -0.10	0.02, -0.09
15	-0.05, -0.04	-0.06, 0.06	1.55, -0.21	-0.01, -0.15	-0.01, 0.09	0.01, 0.00
16	-0.04, 0.00	-0.05, -0.03	1.54, -0.24	-0.02, -0.12	-0.05, 0.01	0.01, 0.05
17	-0.03, 0.10	-0.07, 0.02	1.52, -0.21	-0.03, -0.19	0.07, 0.08	0.05, -0.06
18	-0.04, 0.04	-0.09, -0.05	1.55, -0.24	0.02, -0.22	0.09, 0.05	0.01, 0.03
19	-0.03, 0.09	-0.11, 0.05	1.56, -0.10	-0.02, -0.10	0.08, 0.04	0.07, 0.09
20	-0.04, 0.08	-0.07, 0.02	1.54, -0.07	0.01, -0.15	0.02, 0.07	0.04, -0.11

Effect of Systematic Errors

The table 5 contains data from experimental scenario in Section 5.2, where effects of the camera and the odometry bias were measured.

Table 5: Effect of systematic errors on navigation convergence

Loop	**Position relative to start** [m] *systematic error (bias)* *none*	*camera*	*odom.*	*both*
00	0.00, 0.00	0.00, 0.00	0.00, 0.00	0.00, 0.00
01	0.08, -0.02	-0.30, 0.37	0.08, 0.09	-0.16, 0.28
02	0.02, 0.04	-0.28, 0.39	0.09, 0.13	-0.15, 0.38
03	-0.02, 0.11	-0.35, 0.44	0.13, 0.24	-0.16, 0.46
04	0.10, 0.07	-0.29, 0.38	0.15, 0.30	-0.15, 0.50
05	0.10, 0.11	-0.31, 0.50	0.17, 0.35	-0.03, 0.53
06	0.08, 0.00	-0.33, 0.52	0.13, 0.32	-0.24, 0.49
07	0.01, 0.07	-0.34, 0.49	0.19, 0.30	-0.14, 0.52
08	0.00, -0.01	-0.32, 0.46	0.13, 0.31	-0.18, 0.49
09	-0.01, 0.02	-0.33, 0.49	0.12, 0.30	-0.13, 0.50
10	0.00, -0.04	-0.36, 0.49	0.10, 0.26	-0.14, 0.49
11	-0.04, -0.14	-0.35, 0.50	0.13, 0.39	-0.33, 0.47
12	0.02, -0.02	-0.32, 0.50	0.18, 0.44	-0.39, 0.49
13	0.03, -0.06	-0.35, 0.45	0.13, 0.31	-0.38, 0.48
14	0.06, 0.04	-0.33, 0.49	0.14, 0.34	-0.18, 0.49
15	-0.01, -0.15	-0.32, 0.45	0.14, 0.29	-0.13, 0.50
16	-0.02, -0.12	-0.31, 0.40	0.11, 0.25	-0.12, 0.49
17	-0.03, -0.19	-0.36, 0.44	0.11, 0.29	-0.16, 0.51
18	0.02, -0.22	-0.31, 0.46	0.11, 0.24	-0.15, 0.54
19	-0.02, -0.10	-0.35, 0.42	0.12, 0.26	-0.21, 0.53
20	0.01, -0.15	-0.32, 0.44	0.13, 0.27	-0.12, 0.53

Obstacle Avoidance

The table 6 contains data from the experiment scenario described in Section 5.3, where we verified the method ability to deal with obstacles.

Table 6: Positioning errors with and without obstacles

Loop	**Position relative to start** [m]	
	clear path	*obstacles*
00	0.00, 0.00	0.00, 0.00
01	0.08, -0.02	0.24, 0.22
02	0.02, 0.04	0.12, 0.06
03	-0.02, 0.11	0.17, 0.08
04	0.10, 0.07	0.11, -0.08
05	0.10, 0.11	0.15, -0.08
06	0.08, 0.00	-0.05, -0.07
07	0.01, 0.07	0.14, -0.12
08	0.00, -0.01	0.15, -0.12
09	-0.01, 0.02	0.02, -0.12
10	0.00, -0.04	0.14, -0.07
11	-0.04, -0.14	0.17, -0.13
12	0.02, -0.02	0.20, -0.04
13	0.03, -0.06	0.08, -0.06
14	0.06, 0.04	0.19, -0.03
15	-0.01, -0.15	0.14, -0.03
16	-0.02, -0.12	0.13, 0.04
17	-0.03, -0.19	0.15, -0.03
18	0.02, -0.22	0.02, -0.13
19	-0.02, -0.10	0.17, -0.06
20	0.01, -0.15	0.14, -0.01

Environment and Lighting Changes

The table 7 contains data from the experiment scenario described in Section 5.4, in which the algorithm was tested in an outdoor environment with long-term environment changes.

Table 7: Long-term algorithm reliability

Loop	**Distance to path start** [m]					
	Month					
	Nov	*Dec*	*Jan*	*Feb*	*Mar*	*Apr*
00	1.50	1.50	1.50	1.50	1.50	1.50
01	0.70	0.92	0.90	0.87	0.83	1.15
02	0.30	0.55	0.60	0.50	0.62	0.83
03	0.13	0.38	0.45	0.22	0.28	0.41
04	0.12	0.33	0.38	0.12	0.15	0.39
05	0.03	0.27	0.28	0.18	0.14	0.33
06	0.18	0.20	0.27	0.21	0.09	0.12
07	0.06	0.28	0.22	0.23	0.19	0.07
08	0.09	0.24	0.26	0.24	0.28	0.26
09	0.10	0.29	0.24	0.22	0.23	0.40
10	0.02	0.27	0.28	0.21	0.26	0.38
11	0.23	0.20	0.24	0.22	0.29	0.32
12	0.08	0.20	0.20	0.23	0.23	0.37
13	0.22	0.28	0.20	0.29	0.27	0.27
14	0.14	0.29	0.25	0.27	0.26	0.29
15	0.24	0.29	0.21	0.27	0.11	0.46
16	0.40	0.27	0.24	0.27	0.31	0.28
17	0.42	0.22	0.24	0.22	0.23	0.23
18	0.43	0.23	0.27	0.23	0.15	0.29
19	0.48	0.23	0.23	0.28	0.19	0.35
20	0.45	0.20	0.21	0.28	0.24	0.36

One-day Outdoor Experiment

The table 8 contains data from the experiment scenario 5.5, in which the algorithm was tested in an outdoor environment with variable terrain.

Table 8: One-day Outdoor Experiments

Loop	**Position relative to start** [m]	
	map age	
	up to date	*one week*
00	0.00, 1.50	0.00, 1.50
01	-0.07, 0.03	0.63, 0.15
02	-0.21, 0.18	0.59, 0.11
03	-0.34, 0.15	0.53, 0.17
04	-0.05, -0.14	0.32, 0.19
05	0.34, 0.05	-0.09, 0.22
06	-0.25, 0.06	0.15, 0.20

Landmark Deficiency Experiment

The table 9 contains data from the experiment scenario described in Section 5.6, in which the algorithm was tested during night in low visibility conditions.

Table 9: Landmark deficiency experiment

Loop	**Position relative to start** [m]
00	0.00, 1.50
01	-0.13, -0.29
02	0.21, -0.43
03	-0.09, -0.34
04	-0.32, -0.20
05	0.12, -0.14
06	-0.08, -0.32
07	-0.05, -0.13
08	-0.29, -0.24
09	-0.09, -0.33
10	-0.10, -0.36